Paleoceanography and Paleoclimatology

RESEARCH ARTICLE
10.1029/2024PA004872

Reconciling the Apparent Discrepancy Between Cenozoic Deep-Sea Temperatures From Proxies and From Benthic Oxygen Isotope Deconvolution

E. J. Rohling[1,2], T. M. Gernon[2], D. Heslop[3], G. J. Reichart[4], A. P. Roberts[3], and J. Yu[3,5,6]

[1]Department of Earth Sciences, Utrecht University, Utrecht, The Netherlands, [2]School of Ocean and Earth Science, University of Southampton, Southampton, UK, [3]Research School of Earth Sciences, Australian National University, Canberra, ACT, Australia, [4]Department of Ocean Systems, NIOZ Royal Netherlands Institute for Sea Research, Texel, The Netherlands, [5]Laoshan Laboratory, Qingdao, China, [6]SKLLQG, Institute of Earth Environment, Chinese Academy of Sciences, Xi'an, China

Key Points:

- We quantify major deep-sea temperature discrepancies between benthic foraminiferal O-isotope deconvolutions and clumped isotopes
- We quantitatively evaluate potential explanatory hypotheses, finding that each individually falls short of explaining the discrepancies
- New clumped isotope calibrations, along with carbonate ion or pH changes, can reconcile the discrepancies

Supporting Information:

Supporting Information may be found in the online version of this article.

Correspondence to:

E. J. Rohling,
eelco_rohling@me.com

Citation:

Rohling, E. J., Gernon, T. M., Heslop, D., Reichart, G. J., Roberts, A. P., & Yu, J. (2024). Reconciling the apparent discrepancy between Cenozoic deep-sea temperatures from proxies and from benthic oxygen isotope deconvolution. *Paleoceanography and Paleoclimatology*, *39*, e2024PA004872. https://doi.org/10.1029/2024PA004872

Received 10 FEB 2024
Accepted 16 OCT 2024

Author Contributions:

Conceptualization: E. J. Rohling
Data curation: E. J. Rohling, J. Yu
Formal analysis: E. J. Rohling, J. Yu
Funding acquisition: E. J. Rohling
Investigation: E. J. Rohling, T. M. Gernon, D. Heslop, G. J. Reichart, A. P. Roberts, J. Yu
Methodology: E. J. Rohling, T. M. Gernon, D. Heslop, G. J. Reichart, A. P. Roberts, J. Yu
Project administration: E. J. Rohling
Resources: E. J. Rohling
Software: E. J. Rohling
Validation: E. J. Rohling
Visualization: E. J. Rohling

Abstract Understanding past deep-sea temperature and sea-water oxygen isotope ratios is fundamental to environmental Earth science. For example, it provides crucial insight into past ice-volume variations, an important climate system feedback. Moreover, deep-sea temperature is important to deep-sea ecology and biogeochemical cycling. Here we compare deep-sea temperature and sea-water oxygen isotope ratios from model-based deconvolution of benthic foraminiferal carbonate $\delta^{18}O$ with clumped isotope-based deep-sea temperature data in 1000-year timesteps over the Cenozoic. To assess wider implications of the observed differences, we quantitatively evaluate a range of potential explanatory hypotheses—such as diagenetic overprints, carbonate ion effects, ice-sheet morphology changes, and warm saline deep-water admixture—but find that, individually, none can explain the observed differences satisfactorily. We then evaluate the implications of possible combined effects and recent advances in clumped isotope temperature calibration. We find that combined consideration of a recently proposed cool clumped isotope calibration and possible carbonate ion or pH influences can provide results that approximate deep-sea temperature reconstructions based on conventional $\delta^{18}O_c$ deconvolution. The match can be further improved if modest warm saline deep-water contributions are considered during past warm periods. This contrasts with ice-volume and ice-sheet morphology changes, which appear unrealistic or insignificant, respectively. Our quantitative comparison offers a means toward formulation of a comprehensive and internally consistent understanding of Cenozoic variability in sea level (ice volume), GIA-corrected ice-sheet heights and mean ice $\delta^{18}O$, sea-water $\delta^{18}O$, sea-water $\delta^{18}O_w$, deep-sea temperature, and deep-sea $[CO_3^{2-}]$ variations.

1. Introduction

Past deep-sea water temperature (T_w) can be reconstructed using proxies, notably Mg/Ca ratios and clumped isotopes in benthic foraminiferal carbonate (e.g., Elderfield et al., 2010, 2012; Lear et al., 2004; Meckler et al., 2022; Modestou et al., 2020), or using model-based deconvolutions of stable oxygen isotope records of deep-sea benthic foraminiferal carbonate ($\delta^{18}O_c$; e.g., Bintanja et al., 2005; Bintanja & van de Wal, 2008; de Boer et al., 2010; Hansen et al., 2013; Berends et al., 2021; Rohling et al., 2021, 2022). $\delta^{18}O_c$ records are conventionally thought to have two dominant controls, namely the seawater oxygen isotope ratio ($\delta^{18}O_w$) and T_w-dependent water-to-carbonate oxygen isotope fractionation (here represented in simplified form by $\delta^{18}O_t \approx -0.25T_w$; e.g., Marchitto et al., 2014; Rohling et al., 2021, 2022), so that $\delta^{18}O_c \approx \delta^{18}O_w + \delta^{18}O_t$ (e.g., Berends et al., 2021; Bintanja et al., 2005; Bintanja & van de Wal, 2008; de Boer et al., 2010; Hansen et al., 2013; Rohling et al., 2021, 2022; Shackleton & Opdyke, 1973). Note that, throughout, we express our analyses in terms of changes relative to present (i.e., as relative changes, not absolute values), so that full notation here would be $\Delta\delta^{18}O_c = \Delta\delta^{18}O_w + \Delta\delta^{18}O_t$. We merely omit the Δs to avoid clutter.

Running-average (7-point) Mg/Ca-based deep-sea temperatures of Lear et al. (2004) are largely coherent with deep-sea temperatures obtained from deconvolution of benthic foraminiferal $\delta^{18}O_c$ data with a similar method to that used here (see Figure 16 of Rohling et al., 2022). In other cases, there is a discrepancy between $\delta^{18}O_t$ records inferred from measured $\delta^{18}O_c$ and sea-level/ice-volume-derived $\delta^{18}O_w$, and $\delta^{18}O_t$ data inferred from deep-sea temperature proxies, with both clumped isotopes and Mg/Ca ratios in foraminiferal carbonate indicating more

Writing – original draft: E. J. Rohling, T. M. Gernon, D. Heslop, G. J. Reichart, A. P. Roberts, J. Yu
Writing – review & editing: E. J. Rohling, T. M. Gernon, D. Heslop, G. J. Reichart, A. P. Roberts, J. Yu

elevated deep-sea temperatures in the past (e.g., Leutert et al., 2021; Meckler et al., 2022; Modestou et al., 2020; Rohling et al., 2021, 2022). For example, Modestou et al. (2020) revealed up to ∼6–7°C higher Mg/Ca-based T_w and ∼6–9°C higher clumped isotope-based T_w for the Middle Miocene SE Indian Ocean relative to present, whereas deconvolution of global benthic foraminiferal $\delta^{18}O_c$ only yields up to ∼3–4°C higher T_w values than present (Rohling et al., 2022). Hence, not only proxy-versus-model differences but also proxy-versus-proxy (notably, Mg/Ca vs. clumped isotope) differences may need to be addressed (Leutert et al., 2021) although the difference between Mg/Ca and clumped isotope-based T_w estimates often falls within the generous reported uncertainties; Modestou et al., 2020).

Here we focus on proxy-versus-model comparison, with emphasis on the clumped isotope proxy (e.g., Eiler, 2007; Eiler, 2011; Ghosh et al., 2006), which may have lingering uncertainties in benthic species calibration (e.g., Daëron & Gray, 2023), but which lacks major additional uncertainties as found in the Mg/Ca proxy, related to fluctuations in the deep-water carbonate ion concentration [CO_3^{2-}] (Yu & Elderfield, 2008) and the sea-water Mg/Ca ratio. For the clumped isotope data, we choose to minimize the risk of introducing errors during recalibration between studies and during normalization to modern (core-top) values from the same location and same method, by using a single, uniformly processed data set that temporally spans the Cenozoic (Meckler et al. (2022). However, we add clumped-isotope data from Modestou et al. (2020) and Hou et al. (2023) to fill in major temporal gaps (adjusting the calibrations where necessary). We acknowledge that better-resolved Mg/Ca and clumped isotope records through a brief interval of time (3.36–3.16 Ma) suggest potential deep-water contrasts between the Pacific with an absolute values range of 0–5°C (today, 1.6°C) and the Atlantic with ∼5–10°C (today, 2.6°C) (Braaten et al., 2023), so that the largely Atlantic Meckler et al. (2022) data set might somewhat overestimate global mean values. To judge the importance of this potential offset to our comparison, a major analytical campaign toward improved global coverage over the entire Cenozoic would be needed. Such addition of large numbers of new clumped isotope data would also help to reduce uncertainty in the reconstructed variability through time.

We initially use the clumped isotope temperature data based on the calibration applied in Meckler et al. (2022). Thereafter, we evaluate the potential implications of lower reconstructed temperature values based on the calibration discussed by Daëron and Gray (2023), which is found to result in on average ∼2.2°C lower temperatures over the data set considered. This relatively cold calibration (Daëron & Gray, 2023) relies on planktonic foraminiferal data, and tends to return anomalously low values at the cold end, relative to the "MIT" calibration shown by Daëron and Gray (2023) and broader comparisons in Daëron and Vermeesch (2024). Given that we do not know which calibration is best, and that other published calibrations largely fall between the two used here (e.g., Daëron & Vermeesch, 2024), we instead opt to consider a realistic envelope between the relatively warm Meckler et al. (2022) and relatively cold Daëron and Gray (2023) calibration endmembers.

Next, we use model-based benthic $\delta^{18}O_c$ deconvolution as an internally consistent template for comparison with proxy-based T_w reconstructions. Even if the partitioning between $\delta^{18}O_w$ and $\delta^{18}O_t$ might be challenged, the key to using this template is internal consistency within the $\delta^{18}O_c \approx \delta^{18}O_w + \delta^{18}O_t$ deconvolution that should be maintained unless valid (quantified) reasons can be given against it. That is, if we assume that proxy-based T_w reconstructions are correct, then discrepancies between these values and those from model-based benthic $\delta^{18}O_c$ deconvolution require explanation of why benthic $\delta^{18}O_c$ deconvolution would give different results, which challenges either *(a)* the understanding of Rayleigh Distillation impacts on ^{16}O and ^{18}O during evaporation, atmospheric transport, and precipitation, which derives from $\delta^{18}O$ measurements in both nature and laboratories on evaporating water bodies, vapor, clouds, rain, snow, and ice (e.g., Ellehoj et al., 2013; Jouzel & Merlivat, 1984; Lamb et al., 2017; Majoube, 1970, 1971; Merlivat, 1978; Merlivat & Jouzel, 1979); or *(b)* foundational concepts in paleoceanography about $\delta^{18}O_w$-to-$\delta^{18}O_c$ fractionation (Epstein et al., 1951, 1953; Erez & Luz, 1982, 1983; Harmon & Schwarcz, 1981; Kim & O'Neil, 1997; Marchitto et al., 2014; McCrea, 1950; O'Neil et al., 1969; Rohling & Cooke, 1999; Shackleton, 1974; Shackleton & Opdyke, 1973; Urey, 1947).

Specifically, a major discrepancy raises questions of whether the $\delta^{18}O_c$ measured today is representative of the original shell $\delta^{18}O_c$ (has there been alteration?), whether the conventional view that $\delta^{18}O_c \approx \delta^{18}O_w + \delta^{18}O_t$ might be incorrect (are there other major contributors?), or whether conventional views of the relationship between $\delta^{18}O_w$ and ice-volume changes may be incorrect (was Rayleigh Distillation of oxygen isotopes in precipitation over ice sheets fundamentally different than today, or were there other major influences on $\delta^{18}O_w$ such as major changes in continental groundwater volumes?). To address these questions, we quantify the discrepancy between

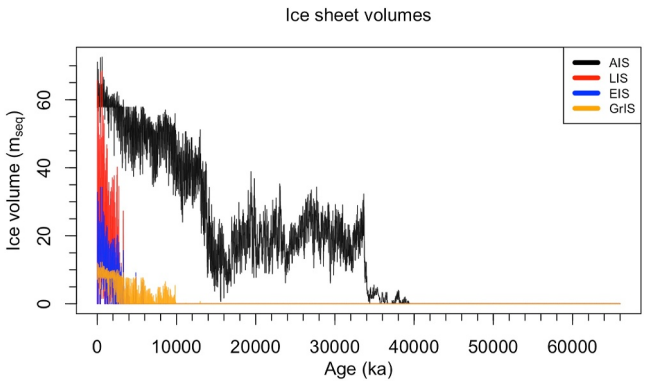

Figure 1. Ice-volume variations (in meters sea-level equivalent; m_{seq}) over the past 66 million years for the four ice sheets considered, following the method of Rohling et al. (2021, 2022).

$\delta^{18}O_t$ records inferred from model-based $\delta^{18}O_c$ deconvolution and $\delta^{18}O_t$ data from deep-sea temperature proxies (notably, clumped isotopes), and calculate the implications of different potential explanatory scenarios; first in a one-by-one approach, and subsequently considering potential combinations. Next, we discuss these implications to eliminate unlikely explanations, and finally we evaluate how recent advances in clumped isotope paleotemperature reconstruction help to address the perceived discrepancies.

Similar to the deep-sea clumped isotope data used in this study (above), the Cenozoic $\delta^{18}O_c$ record used here (Westerhold et al., 2020) has considerable Atlantic bias. Hence, our findings are primarily applicable to the Atlantic domain. Yet, given that we consider all variability after normalization to present-day (core-top) values, we contend that the long-term patterns we discuss are likely to have been largely homogenized throughout the global ocean. The normalization we apply in addition avoids the need for conversion calculations between $\delta^{18}O$ variations in carbonates that are measured versus the Vienna PeeDee Belemnite (VPDB) standard and $\delta^{18}O$ variations in water, vapor, and ice that would be measured versus the Vienna Standard Mean Ocean Water (VSMOW) standard. Despite offsets between absolute values on these scales, relative variations are similar within 3%, given that $\delta^{18}O_{VSMOW} = 1.03092\ \delta^{18}O_{VPDB} + 30.92$ (Coplen et al., 1983; NIST, 1992; Rohling & Cooke, 1999).

Finally, we emphasize that this study does not pretend to offer a final solution to the observed discrepancies. Instead, it provides a first-order quantification of the discrepancies, and quantitatively evaluates the likelihood (or not) of possible explanations, including uncertainty propagation. This allows several suggested explanations to be rejected, while highlighting others as targets for further investigation.

2. Approach and Results

2.1. Framework

To portray the general relationship between changes in ice volume and global mean $\delta^{18}O_w$, we use ice-volume histories after Rohling et al. (2021, 2022) (Supporting Information S1). These essentially stipulate that sea-level changes below present-day sea level are dominated by the relatively low-latitude Laurentide and Eurasian ice sheets (LIS and EIS), and that sea-level changes above present-day level are dominated by changes in the high-latitude Greenland and especially Antarctic ice sheets (GrIS and AIS) (Figure 1, Figure S1 in Supporting Information S1). No matter how volume changes are partitioned within these ice-sheet pairs, the mean ice-elevation implications for each pair are relatively robust. That is, assuming that Rayleigh Distillation of oxygen isotopes over ice sheets is adequately understood, the major $\delta^{18}O_w$ trend relative to ice volume can be reasonably approximated.

A caveat in the application of this method for determining $\delta^{18}O_w$ changes from past records of $\delta^{18}O_c$ fluctuations (relative to present) is that sea-level/ice-volume history is first estimated from a Pleistocene convex $\delta^{18}O_c$: sea-level relationship (Rohling et al., 2021, 2022; with the relationship first described by Spratt & Lisiecki, 2016). While precise validity of extrapolation of this relationship into more ancient times cannot be guaranteed, its nature is theoretically robust (Figure 17 of Rohling et al., 2022) and plausible extrapolation uncertainties (at 1σ) have been evaluated at ≤±10 m for sea levels between 0 and +65.1 m (Figure 6 of Rohling et al., 2022), which is ≤±0.1–0.13‰ in $\delta^{18}O_w$ for different ice-sheet morphologies in the present study (below). Note that values are unlikely to fluctuate randomly within these bounds from timestep to timestep, but rather would follow systematic, long-term autocorrelated deviations related to potential long-term changes in ice-sheet properties (cf. Figure 18 of Rohling et al., 2022).

We use the same lens-shaped ice-sheet morphologies with parabolic radial profiles as used by Rohling et al. (2021, 2022). Different from those studies, however, we here also calculate the glacio-isostatic adjustment (GIA) history of bedrock beneath ice sheets (Supporting Information S1) following van den Broek (2006; their Figures 6.1 and 6.3) and de Boer et al. (2010) (Supporting Information S1). In addition, we here include the largely ice-free period between 40 and 66 Ma. Initial ice-free continent shapes are set to be conical, after de Boer et al. (2010) (Table 1). The calculated position/height of each ice-sheet summit and GIA-related bedrock

Table 1
Initial Bedrock Height and Slope for the Continents on Which the Model Grows Ice, and Relaxation Timescale and Density Ratio Used in the GIA Approximations (After de Boer et al., 2010)

	AIS	LIS	EIS	GrIS
Initial bedrock peak height (m asl)	1,270	1,400	1,250	800
Initial bedrock slope	0.001	0.0017	0.0016	0.0014
Asthenosphere relaxation timescale (ky)	3	3	3	3
Density ratio bedrock and ice	3	3	3	3

depression, relative to present-day sea level, are shown in Figures 2a–2d. *X*-axis scales vary between plots because only time intervals with notable variability are shown. When no ice sheet is present, bedrock eventually relaxes toward the initial position (Table 1). A zoomed-in portion of Figure 2b is shown in Figure S2 of Supporting Information S1, to demonstrate in detail the timing-offset between changes in LIS summit height and bedrock position, which is obscured when plotting lines over long timescales in Figure 2b. Using the radial ice-height and GIA-depressions related to the summit values shown in Figures 2a–2d, mean ice elevations are calculated through time for each ice sheet. These mean ice elevations are corrected for sea-level changes because sea-level lowering causes a relative continental ice-elevation increase, and vice versa.

Sea-level-corrected mean ice elevation for each ice sheet is used in stable O-isotope Rayleigh Distillation equations (Supporting Information S1), which are based on thermodynamic first-principles assessments and observations in vapor, precipitation, snow, ice, and cloud environments as well as laboratory experiments (e.g., Ellehoj et al., 2013; Jouzel & Merlivat, 1984; Lamb et al., 2017; Majoube, 1970, 1971; Merlivat, 1978; Merlivat & Jouzel, 1979). This approach of calculating the $\delta^{18}O$ of precipitation over ice sheets replaces the phenomenological approximations used by Rohling et al. (2021, 2022). Based on the new $\delta^{18}O$ of precipitation values, we

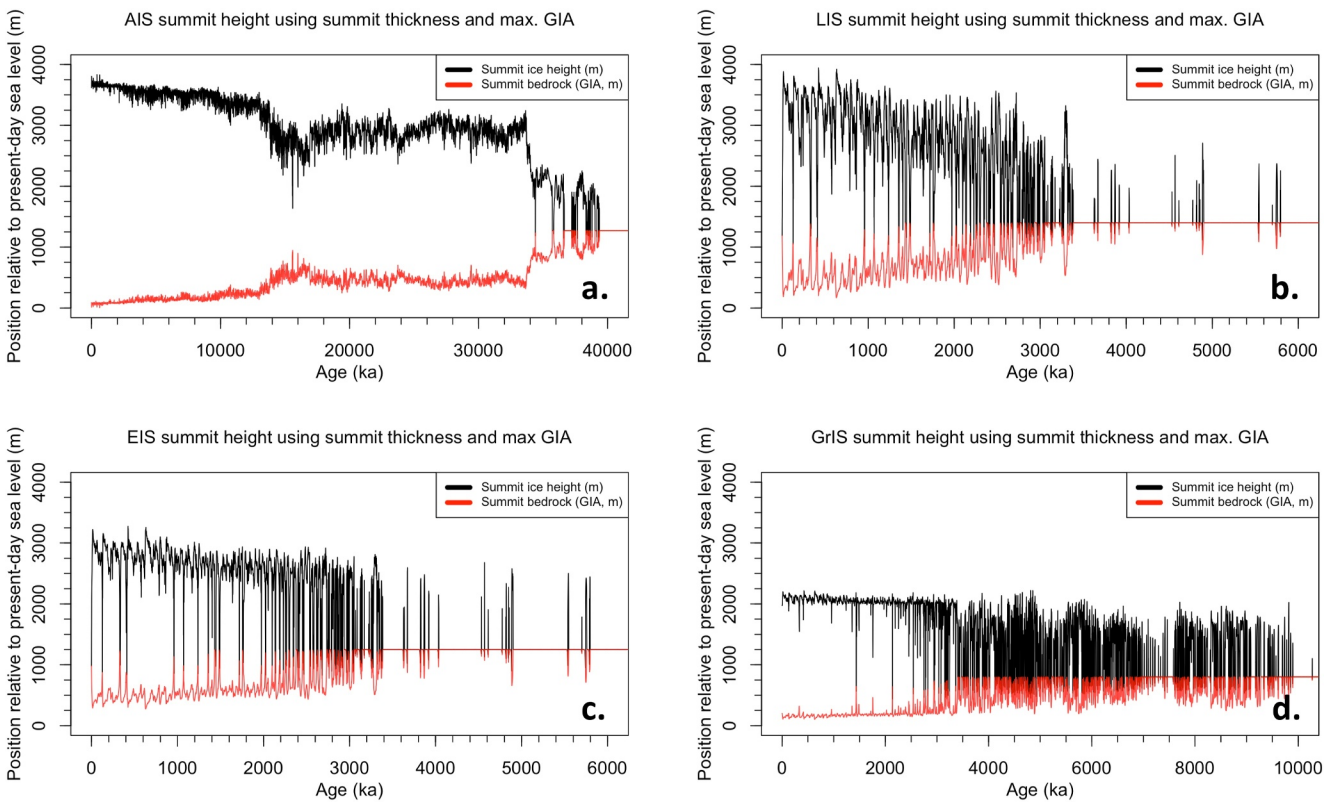

Figure 2. Reconstructed summit heights of the four major ice sheets (i.e., at the center for the radially symmetric ice sheet morphologies considered) and vertical bedrock displacements at that location for our main experiment with relatively steep ice-sheet morphologies (using an aspect ratio similar to that of the modern AIS). The distance between the two curves in each panel indicates the maximum ice-sheet thickness. (a) AIS. (b) LIS. (c) EIS. (d) GrIS.

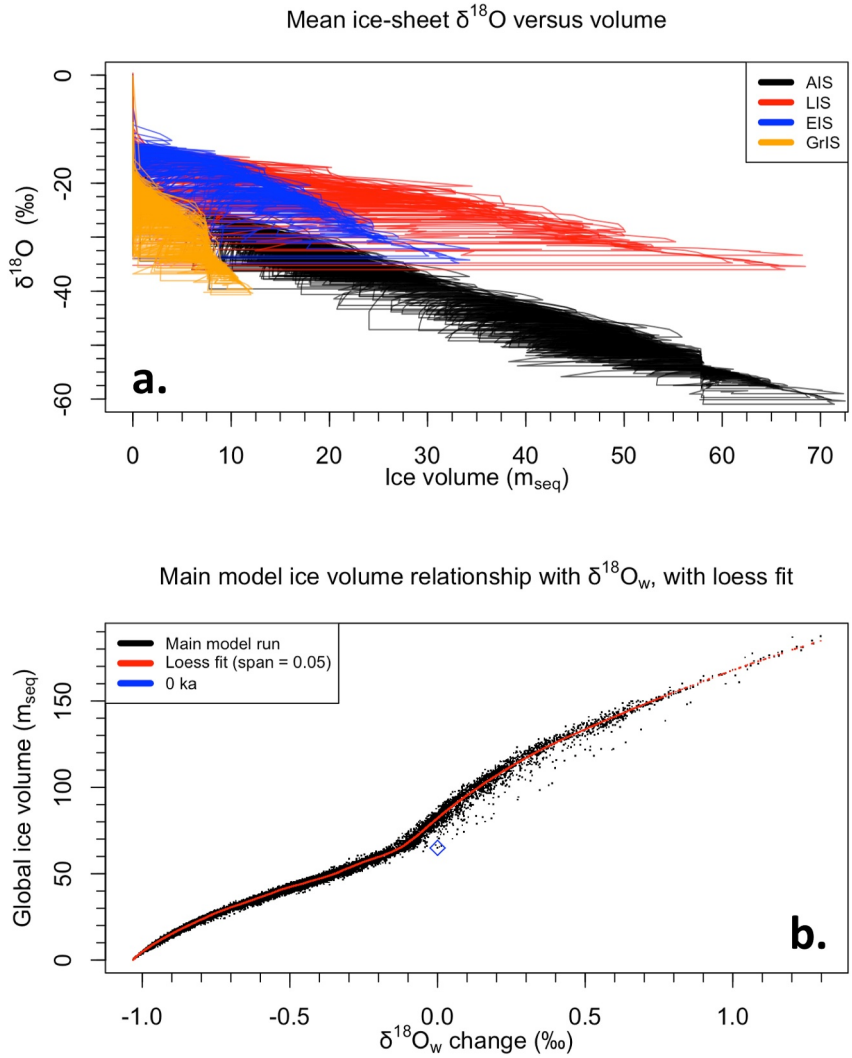

Figure 3. (a) Reconstructed mean ice-sheet $\delta^{18}O$ versus ice volume through time for each of the four ice sheets considered in the main model experiment. (b) Global ice volume (in m_{seq}) versus mean global sea-water $\delta^{18}O$ (i.e., $\delta^{18}O_w$) in the main model run, with loess fit (span = 0.05) that allows approximate model inversion so that global ice volume can be determined from any given $\delta^{18}O_w$.

determined histories of mean ice-sheet $\delta^{18}O$ as in Rohling et al. (2021, 2022) (Figure 3a) for each ice-sheet, and the resultant record of total (all ice-sheet) mean sea-water $\delta^{18}O_w$ (Figure 3b). Under the conventional $\delta^{18}O_c$ deconvolution assumption, this allows calculation of changes in $\delta^{18}O_t$ ($\approx -0.25T_w$) using $\delta^{18}O_t = \delta^{18}O_c - \delta^{18}O_w$. As mentioned before (*Introduction*), full notation would be $\Delta\delta^{18}O_t = \Delta\delta^{18}O_c - \Delta\delta^{18}O_w$, but we omit the Δs to avoid clutter.

In Figure 3b, global ice volume is shown relative to global mean $\delta^{18}O_w$, and a locally estimated scatterplot smoothing (loess) fit (span = 0.05) provides an approximation of the general relationship shape. This loess fit effectively allows inversion of the $\delta^{18}O_c$ deconvolution method including reasonable partitions between low- and high-latitude ice sheets, with limited sensitivity to initial sea-level assumptions, and including GIA influences on mean ice-surface elevation and, thus, on Rayleigh Distillation of O isotopes in precipitation. The loess fit thus provides a means to test the implications of clumped isotope derived T_w data.

Given the conventional concept that, in terms of relative changes, $\delta^{18}O_c \approx \delta^{18}O_w + \delta^{18}O_t$, we can test two extreme scenarios. We can: *(a)* determine implied $\delta^{18}O_c$ values for proxy-based $\delta^{18}O_t$ reconstructions assuming that ice volume (sea level) and $\delta^{18}O_w$ are understood reasonably; or *(b)* determine the implied $\delta^{18}O_w$ (hence, ice

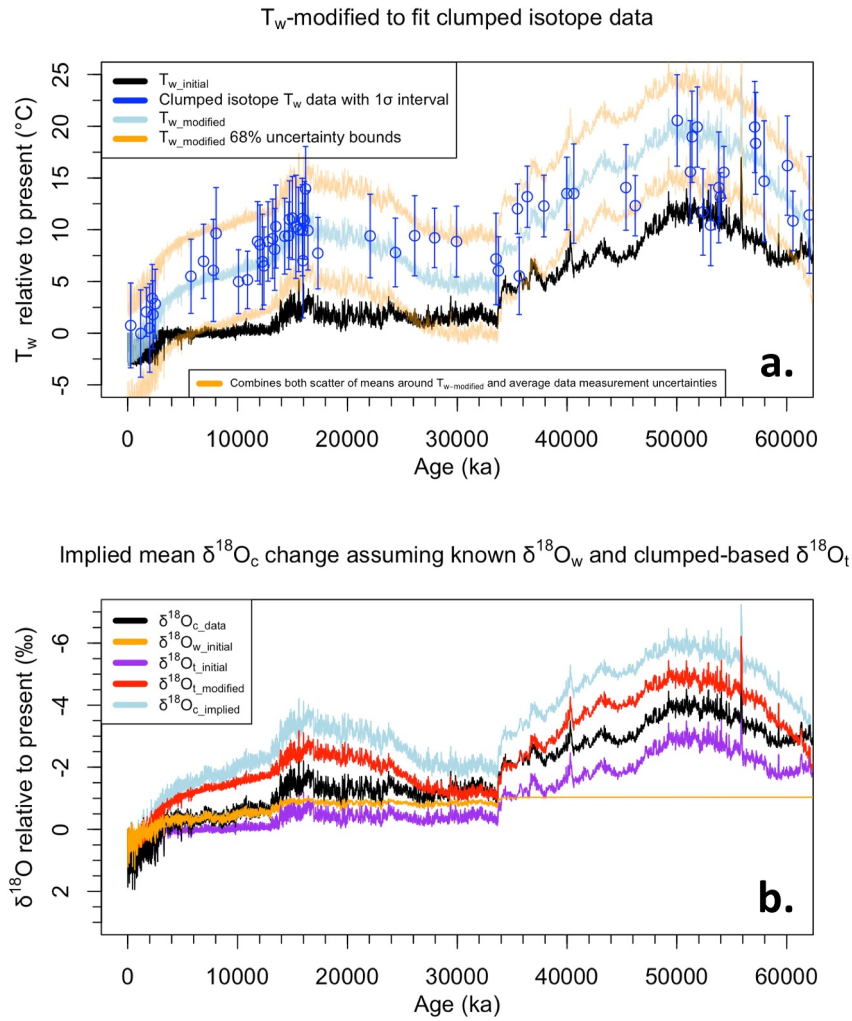

Figure 4. (a) Clumped isotope based T_w data relative to the present (blue open dots with 68% uncertainty intervals; Meckler et al. (2022), Modestou et al. (2020), and Hou et al. (2023)) compared with T_w from the main model's conventional benthic foraminiferal $\delta^{18}O_c$ deconvolution (black), and a version of the black curve perturbed with a long-term empirical polynomial fit (light blue) that offers a reasonable visual long-term fit through the clumped isotope based T_w data, with 68% uncertainty interval (orange). (b) Implied $\delta^{18}O_c$ under the assumptions of scenario (*a*), for the hypothesis that $\delta^{18}O_c$ is insufficiently understood. "Initial" stands for model results from conventional benthic foraminiferal $\delta^{18}O_c$ deconvolution, "modified" for records after modification of the initial record based on the clumped isotope data, and "implied" for the resultant $\delta^{18}O_c$ record.

volume) for proxy-based $\delta^{18}O_t$ reconstructions assuming that measured $\delta^{18}O_c$ records adequately reflect past conditions (i.e., they are not affected by influences other than $\delta^{18}O_w$ or $\delta^{18}O_t$). As outlined before, we first focus on the clumped isotope deep-sea temperature record based on the calibration used in Meckler et al. (2022), and later apply the cooler, planktonic foraminifer-based, clumped isotope calibration from Daëron and Gray (2023). The record based on the calibration from Meckler et al. (2022) yields past T_w values (blue circles) that are considerably higher than the T_w values obtained from conventional $\delta^{18}O_c$ deconvolution (black line) (Figure 4a). For the sake of evaluating the large-scale implications, we construct a hypothetical high-resolution fit (light blue in Figure 4a) through the clumped isotope T_w data by adding short-term T_w variability from our conventional deconvolution run to a long-term smoothing fit through the low-resolution clumped isotope data. This smoothing is obtained using a polynomial to present a reasonable visual fit (see R scripts and Supporting Information S1), given that it serves only to indicate first-order quantitative implications of the contrast between clumped isotope T_w and that from $\delta^{18}O_c$ deconvolution, rather than a precise paleo-reconstruction.

The thus constructed record of clumped isotope-inspired T_w changes is then translated into a record that we term $\delta^{18}O_{t\_modified}$ (Figure 4b, red). We check the notable Mio-Pliocene shift inferred in Figure 4a using additional data. Based on clumped isotope data with the same calibration as Meckler et al. (2022) and additional Mg/Ca results, Braaten et al. (2023) calculated that T_w at 3.36–3.16 Ma was on average 1–2°C higher than present in the eastern equatorial Pacific and ~4.5°C higher than present in the North Atlantic. On average, this corroborates the marked Pliocene upward mean $T_{w\_modified}$ bulge to ~2.5°C (light blue in Figure 4a) and, thus, the related mean $\delta^{18}O_{t\_modified}$ bulge (red in Figure 4b), but also emphasizes the need for more global data coverage.

2.2. Scenario Testing: Main Experiment

The main experiment considers clumped isotope data using the same calibration as Meckler et al. (2022). First, we evaluate scenario (a), estimating implied $\delta^{18}O_c$ values for proxy-based $\delta^{18}O_t$ reconstructions assuming that sea level and $\delta^{18}O_w$ are understood reasonably (Figure 4b). We show the (normalized) measured $\delta^{18}O_c$ data (black), the conventional deconvolution-based $\delta^{18}O_w$ record (orange, labeled "initial" because it derives from the initial deconvolution before clumped isotopes were considered), and the resultant initial $\delta^{18}O_t$ record (purple). We then show the clumped isotope-based $\delta^{18}O_{t\_modified}$ record (red) and calculate the $\delta^{18}O_{c\_implied}$ record (light blue = orange + red). This $\delta^{18}O_{c\_implied}$ would be what $\delta^{18}O_c$ should have looked like under the stated assumptions of this scenario. The difference between $\delta^{18}O_{c\_implied}$ (light blue) and $\delta^{18}O_c$ (black), which is of the order of 1.5–2‰, would then reflect processes other than those conventionally considered in the sum $\delta^{18}O_c \approx \delta^{18}O_w + \delta^{18}O_t$. In the discussion, we evaluate these potential processes in terms of benthic foraminiferal $\delta^{18}O_c$ sensitivity to deep-water carbonate ion concentration or pH (Figures 5a and 5b; Figures 6a–6c).

Next, we evaluate scenario (b), estimating the implied $\delta^{18}O_w$ and therefore ice-volume (sea-level) values for proxy-based $\delta^{18}O_t$ reconstructions assuming that measured $\delta^{18}O_c$ records adequately reflect past conditions; that is, that they were not affected by influences other than $\delta^{18}O_w$ or $\delta^{18}O_t$ (Figure 7a). Again, we show (normalized to their most recent value) the measured $\delta^{18}O_c$ data (black), the conventional (initial) deconvolution-based $\delta^{18}O_w$ record (orange), and the resultant initial $\delta^{18}O_t$ record (purple), and the clumped isotope-based $\delta^{18}O_{t\_modified}$ record (red). We then calculate the $\delta^{18}O_{w\_implied}$ record (light blue = black minus red), which indicates what the ice-volume/sea-level related global seawater $\delta^{18}O$ changes would need to have been under the stated assumptions of this scenario. The $\delta^{18}O_{w\_implied}$ record can be used with the loess fit of Figure 3b (within its constraining data range) to determine implied ice-volume variations (Figure 7b). Uncertainties are based on propagation of the 68% uncertainty bounds to $T_{w\_modified}$ in Figure 4a. In Figure 7b, ice-volume reconstructions for the clumped isotope-based T_w experiment "saturate" at around +185 m_{seq} because that is the constraining data limit for the loess fit. Because of the high clumped isotope T_w values (Figure 4a), this experiment indicates extreme ice volumes (equivalent to Pleistocene glacial maxima) throughout most of the Cenozoic, even including the Paleocene-Eocene greenhouse state (Figure 7b).

It is also possible that there have been major influences on $\delta^{18}O_w$ variation other than ice-volume change. Variations in continental groundwater volumes might be considered, but given that groundwater $\delta^{18}O$ is closely related to precipitation $\delta^{18}O$ (in ice free regions, this is generally much more positive than ice-sheet $\delta^{18}O$), these volume variations would have had to have been considerably larger than the inferred continental ice-volume variations. For example, with ice-volume $\delta^{18}O$ easily of the order of −30‰ (Figure 3a) and median groundwater $\delta^{18}O$ of the order of −10‰ or more positive when excluding snow and ice-bound regions (Jasenchko et al., 2014), ground-water volume fluctuations would need to be three or more times larger than glacial water-volume fluctuations to have similar impacts on $\delta^{18}O_w$. Hence, we consider it unlikely that the entire inferred discrepancy could be explained in terms of continental groundwater fluctuations.

Oxygen isotope exchange changes between the ocean and lithosphere could also introduce long-term $\delta^{18}O_w$ shifts (e.g., Huntington & Petersen, 2023; Meckler et al., 2022; Rohling et al., 2022), but seafloor spreading and production rate changes were relatively small, notably over the last 40 Myr (Gernon et al., 2021; Matthews et al., 2016; Rohling et al., 2022; Young et al., 2019), although recent results indicate a crustal production decrease of 30%–40% from ~15 Ma until 5 Ma (Herbert et al., 2022). The latter study, however, suggests that crustal production is a proxy for tectonic CO_2 degassing, and modeling under that condition indicates that $\delta^{18}O_w$ (including any ice sheets) is unlikely to have varied more than ±1‰ even over the entire Phanerozoic (Coogan et al., 2019). This process is, therefore, unlikely to have played a substantial role in $\delta^{18}O_w$ change, whereas clumped isotope data suggest major deviations from deconvolution-based T_w even in the Pliocene (Figure 4a),

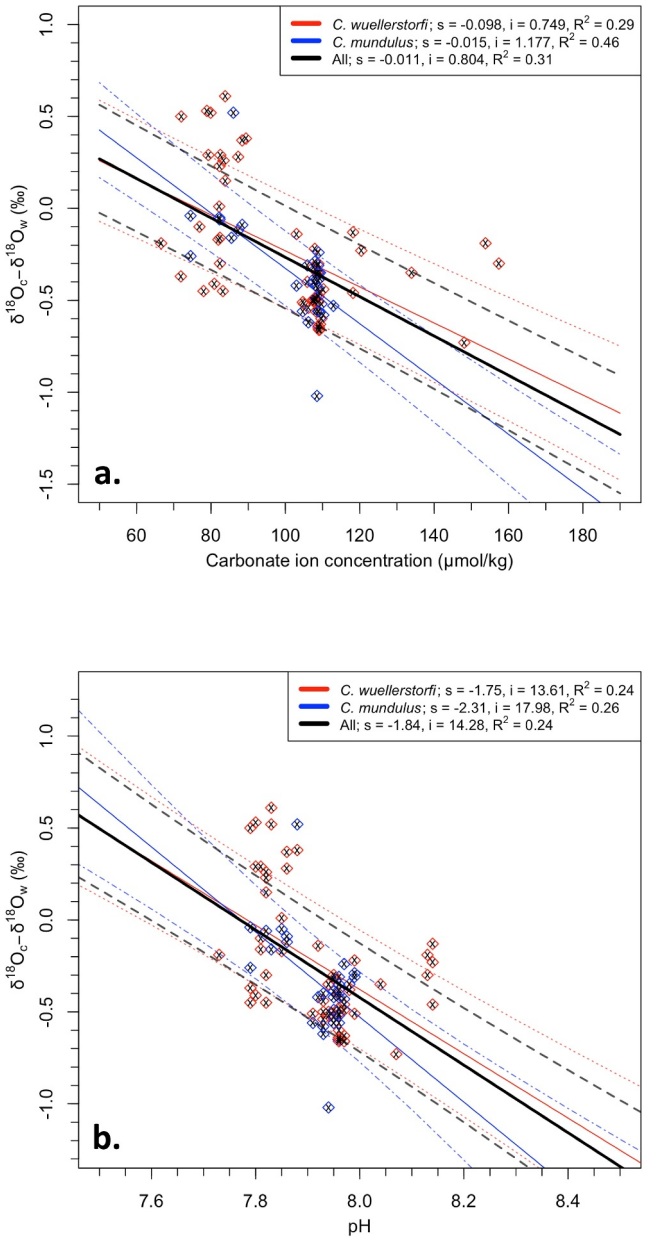

Figure 5. (a) Offset in core top data between benthic foraminiferal $\delta^{18}O_c$ and $\delta^{18}O_w$ relative to deep-water carbonate ion concentrations, for *C. wuellerstorfi* (red) and *C. mundulus* (blue) and all combined (black). For all regressions, 68% prediction intervals are indicated with dashed lines. (b) Similar to panel (a) but with respect to pH. Regressions are ordinary least squares regressions and oxygen isotope offsets on the *Y* axis have been temperature corrected (see Supporting Information S1). In the legend, "s" stands for slope, and "i" for intercept.

which imply dramatic $\delta^{18}O_w$ changes (up to 1.5–2‰) by the Pliocene and before (Figure 7a). Hence, we hereafter ignore changes in oxygen isotope exchange between the ocean and lithosphere for the time-interval studied.

A further suggestion that can be tested is that large deep-sea $\delta^{18}O_w$ variations may be related to changes from warm saline deep water (WSDW) in certain periods to cold less-saline deep water in other periods (Meckler et al., 2022). To test this, we take guidance from extreme conditions in the modern ocean. First, active WSDW formation occurs today in the Red Sea and Mediterranean Sea. In the Red Sea, the freshwater budget is dominated by evaporation, given that runoff and direct precipitation into the basin are negligible. Red Sea salinities reach more than 40 psu, and the Red Sea surface-water $\delta^{18}O_w$:S slope is ~0.3‰ psu^{-1} (Rohling, 1994) (although salinity based on modern relative conductivity measurements is dimensionless, we refer to "practical salinity units" or psu for clarity of presentation in the considered ratios). In the modern Mediterranean, with high evaporation but also substantial runoff and precipitation, salinities reach 39 psu, and the $\delta^{18}O_w$:S slope is similar to that in the Red Sea, at 0.28‰ psu^{-1} (Pierre, 1999; Pierre et al., 1986; Rohling & Bigg, 1998). Second, cold and relatively low-salinity deep-water formation characterizes the open ocean during the Holocene interglacial and the Last Glacial Maximum. Today, typical mean $\delta^{18}O_w$:S slopes throughout the North Atlantic are ~0.6‰ psu^{-1} (Rohling & Bigg, 1998), while mean Arctic outflow (East Greenland Current) ranges between ~0.4 and ~0.8‰ psu^{-1} (Cox et al., 2010). A modern extratropical $\delta^{18}O_w$:S slope of ~0.6‰ psu^{-1} is recognized throughout the ocean (Bigg & Rohling, 2000; Craig & Gordon, 1965), and may have increased to ~1‰ psu^{-1} during the Last Glacial Maximum (LGM; e.g., Adkins & Schrag, 2000; Adkins et al., 2002; Wadley et al., 2002; Miller et al., 2015). The ~0.3‰ psu^{-1} slope under strongly evaporative conditions is robust because the net $\delta^{18}O$ fractionation due to evaporation is about −10‰ relative to surface water, which dominates the net freshwater endmember with (S, $\delta^{18}O$) = (0, −10) versus observed marine endmembers of (39, 1) or (39.5, 1.5). The steeper slopes observed during cold periods are due to net freshwater endmembers with lower $\delta^{18}O$, mainly because of important snow and ice-melt contributions (e.g., Cox et al., 2010). Deviation from the modern $\delta^{18}O_w$:S slope in the ocean toward more evaporative climate conditions that create the potential for WSDW formation, therefore, are likely associated with decreasing $\delta^{18}O_w$:S slopes, down to an evaporation-dominated extreme of ~0.3‰ psu^{-1}.

Mediterranean and Red Sea saline deep waters today are some 3–4 psu more saline than surface waters. Modern open oceanic cold deep waters have relatively similar salinities relative to surface water. If we use modern cold, relatively low-salinity deep-water as a reference, and assume a generous 5 psu deep-water salinity increase for WSDW (which implies that global mean salinity would approach 40 psu, similar to the Mediterranean and Red Sea), then the evaporative effect can impart a rough maximum of $5 \times 0.3 = 1.5$‰ of deep-water $\delta^{18}O_w$ difference (increasing values with a greater WSDW proportion). Assuming a linear $\delta^{18}O_w$:S slope change between the extremes of cold, less saline deep water and WSDW (i.e., mixing between only two fundamental components), the $\delta^{18}O_{w\_implied}$ record (Figure 7a) can be translated into a WSDW percentage contribution to global deep water (Figure 7c). We perform this calculation relative to $\delta^{18}O_w$ from the main model experiment (orange in Figure 7a). Uncertainties are based on propagation of the 68% uncertainty bounds to $T_{w\_modified}$ in Figure 4a. This is a crude comparison, which focuses only on potential long-term WSDW implications (long-term fits) (Figure 7c).

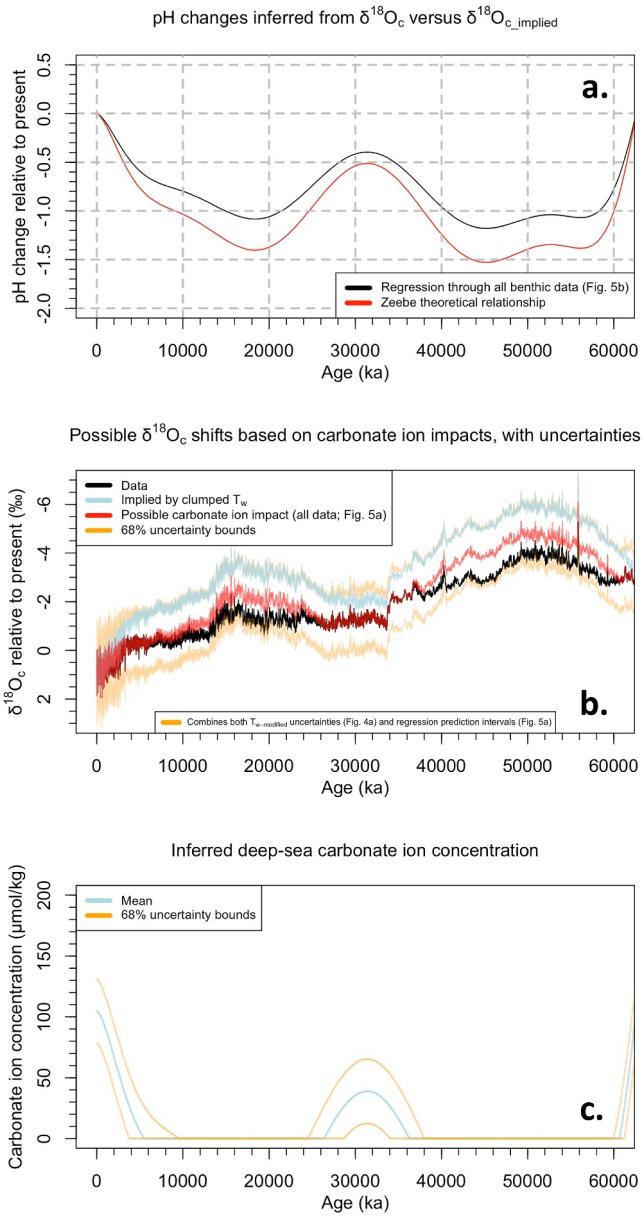

Figure 6. (a) Implied pH changes (relative to present) for scenario (*a2*) in our main experiment with relatively steep ice-sheet morphologies. Black is based on the slope of the regression through all data in Figure 5b. Red is based on the slope of the theoretical relationship discussed in Zeebe (1999, 2001). (b) Inferred adjustment from the $\delta^{18}O_c$ that would have been deposited originally based on clumped isotope T_w reconstruction (light blue), toward the $\delta^{18}O_c$ that is measured on the benthic foraminifera (black), given the $[CO_3^{2-}]$ bounds discussed in the text. Red is the mean based on the regression through all data in Figure 5a, and orange delineates the fully propagated 68% uncertainty interval. (c) Inferred $[CO_3^{2-}]$ changes through time based on assessment of carbonate ion effects in scenario (*a2*) in our main model run with clumped isotope calibration as in Meckler et al. (2022) and relatively steep ice-sheet morphologies.

Finally, combined effects are considered (for all experiments). Here we allow for the maximum carbonate ion-related shift in $\delta^{18}O_c$, which yields the red line in Figure 6b, and determine the remaining offsets with respect to measured $\delta^{18}O_c$ data (black in Figure 6b). We then translate these into implied changes in either WSDW contributions or ice-volume (Figures 8a and 8b). Uncertainties are based on propagation of the 68% uncertainty bounds (orange) around the red record in Figure 4a.

2.3. Additional Experiments

Next, we test implications of potential changes in the height/radius aspect ratio of ice sheets. The aspect ratio is essentially a function of bed friction (Bailey et al., 2010; Clark & Pollard, 1998; Willeit et al., 2019). In the main experiment, we assumed that ice-sheet morphology always had the same aspect ratio, which was selected based on the present-day AIS (Rohling et al., 2021, 2022). However, the so-called regolith hypothesis proposes that early ice sheets, which formed when there was still a substantial regolith cover on the continents, formed with lower bed friction and, thus, had a lower aspect ratio (Clark & Pollard, 1998; Willeit et al., 2019). Such ice sheets have been named "low-slung, slippery ice sheets" (Bailey et al., 2010). To explore the impacts of a lower aspect ratio on our results, we ran a new experiment with the same ice-volume histories, but with an ice-sheet aspect ratio that is half that used in the main experiment, and produced the same suite of figures (Figures S3–S7 in Supporting Information S1). Since there is no conclusive information on when, and to what extent, the aspect ratio of the ice sheets may have changed, we present solutions for low-slung slippery ice sheets throughout the interval of study (Figures S3–S7 in Supporting Information S1), for comparison with the steeper ice-sheet main-experiment results (Figures 1–7).

Finally, we repeated all of the above using lower clumped-isotope T_w values, based on the planktonic foraminiferal clumped isotope calibration of Daëron and Gray (2023) (Figures 9 and 10; Figures S8 and S9 in Supporting Information S1). In Figures 9 and 10, we consider implications of the cooler clumped-isotope calibration while maintaining the steep ice-sheet aspect ratio of the main experiment. In Figures S8 and S9 of Supporting Information S1, we consider implications of a combination of cooler clumped-isotope calibration with a reduced ice-sheet aspect ratio (low-slung ice sheets).

Below, we discuss the various tests on an individual basis, followed by clumped isotope calibration implications, and the impacts of combined influences.

3. Discussion

3.1. Hypothesis That $\delta^{18}O_c$ Is Understood Insufficiently

Scenario (a), portrayed in Figure 4b, suggests either (*a1*) that $\delta^{18}O_c$ would need to have been markedly different when the benthic foraminifera were forming their shell carbonate than the $\delta^{18}O_c$ measured on these shells today, or (*a2*) that additional factors exist that control $\delta^{18}O_c$, which caused the difference to be locked in during shell carbonate deposition.

In case (*a1*), diagenetic effects within sediments are the most likely culprit. However, Leutert et al. (2019) state: *"We find that overall, primary Δ_{47}* [i.e., clumped isotope] *signatures appear similarly sensitive to diagenetic overprinting as $\delta^{18}O$, with differences in sensitivity depending on pore fluid chemistry and the amount of secondary calcite. … The Δ_{47} and $\delta^{18}O$ values of*

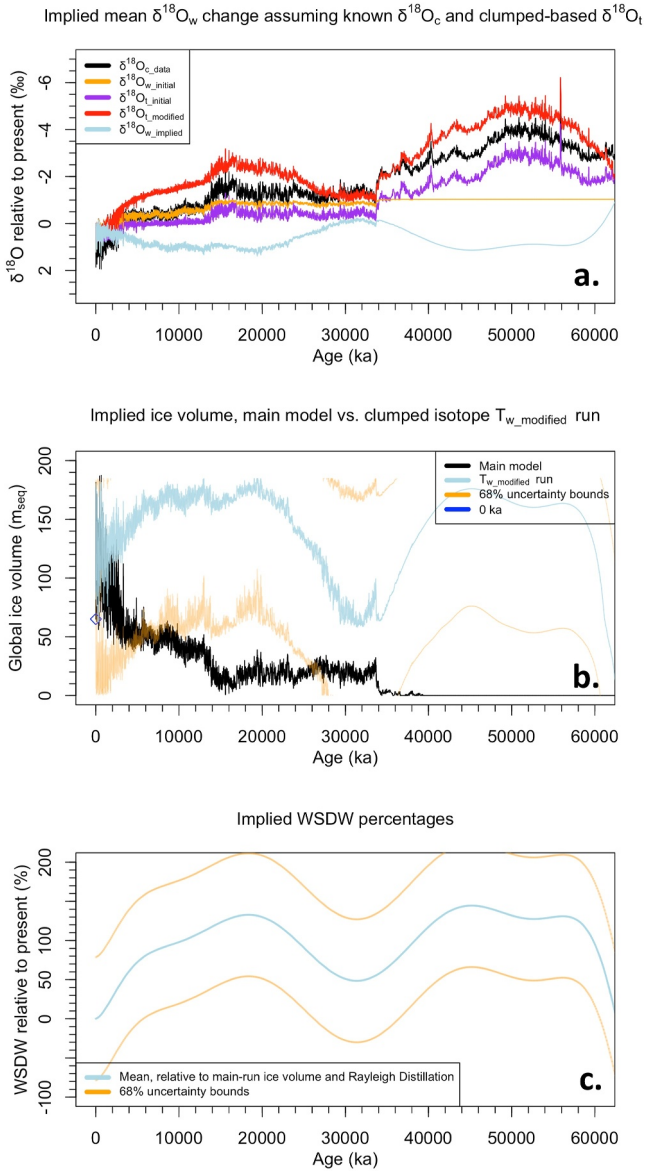

Figure 7. (a) Implied $\delta^{18}O_w$ under the assumptions of scenario (b), for the hypothesis that $\delta^{18}O_w$ and/or ice volume are insufficiently understood. "Initial" stands for model results from conventional benthic foraminiferal $\delta^{18}O_c$ deconvolution, "modified" for records after modification of the initial record based on the clumped isotope data, and "implied" for the resultant $\delta^{18}O_w$ record. (b) Implied ice volume, relative to present, if scenario (*b*) is fully ascribed to a poorly understood ice-volume history. Black indicates the main experiment-based ice volume, light blue the ice volume based on the mean clumped-isotope-based T_w (Figure 4a), and orange the 68% uncertainty levels. (c) Implied WSDW percentages, relative to the present, for the hypothesis that (implied) large $\delta^{18}O_w$ variations can be explained in terms of the $\delta^{18}O_w$ contrast between warm saline deep water and cold, less saline deep water. Light blue and orange as in (b).

benthic … foraminifera are less affected by diagenesis and thus likely to yield robust foraminiferal calcification temperatures" (see also Huntington & Petersen, 2023). Note that hypothesis *a1* would require virtually complete recrystallization within sediments at temperatures up to 6–8°C *lower* than bottom-water temperatures (offsetting the difference between $T_{w\_modified}$ and T_w in Figure 4a). For only partial (e.g., 1/3) recrystallization, within-sediment temperatures would need to have been even lower (roughly 3× the offset in the example above) to achieve the same weighted mean result. This seems unlikely, as temperatures within sediments are more likely to be *higher* due to the geothermal gradient. Moreover, we emphasize, following Leutert et al. (2019) that such large-scale recrystallization at substantially different temperatures would have shifted clumped isotope temperatures as well as $\delta^{18}O_c$.

In case (*a2*), changes in bottom-water carbonate ion concentrations (i.e., $[CO_3^{2-}]$, a function of pH) would be the most likely culprit (Meckler et al., 2022), causing (part of) the up to 1.5–2‰ offset between $\delta^{18}O_{c\_implied}$ from clumped isotopes and measured $\delta^{18}O_c$ (light blue and black in Figure 4b). To assess this, we obtained new species-specific epifaunal benthic foraminiferal data (*C. wuellerstorfi* and *C. mundulus*) from global core-top sediments and find that, for the combined data set, $\delta^{18}O_c - \delta^{18}O_w = -0.011$ $[CO_3^{2-}]$–0.804, or $\delta^{18}O_c - \delta^{18}O_w = -1.84pH–14.28$, both with 68% prediction intervals of the order of ± 0.35‰ (black solid and dashed lines in Figures 5a and 5b). Using linear extrapolation, we back-calculate pH change relative to present, based on the shift (in a positive direction) inferred from $\delta^{18}O_{c\_implied}$ to the measured $\delta^{18}O_{c\_data}$, using either the regression-based slope (Figure 5b) or the theoretical −1.42‰ per pH unit of Zeebe (1999, 2001) (Figure 6a). The pH-change calculation is slope-dependent only, so that it is not straightforward to propagate the prediction intervals. Moreover, the linearity of extrapolation in pH space may be questioned, given that planktonic foraminiferal $\delta^{18}O_c$ relates non-linearly to pH in cultures, in contrast to an approximately linear relationship with $[CO_3^{2-}]$ (Bijma et al., 1999). Unfortunately, data scatter and limited coverage of natural data along the ranges of the *X*-axes in Figure 5 preclude detection of any non-linearity. With these caveats in mind, and noting that our approach can yield smooth long-term changes only because short-term variability was kept the same between T_w and $T_{w\_modified}$ (hence, only the long-term T_w adjustment to fit clumped isotope data affects the solution), calculated pH changes seem excessive through most of the Cenozoic, even exceeding −1 pH unit (Figure 6a).

For $[CO_3^{2-}]$ (Figure 6b), we followed a different approach and calculate the largest possible $[CO_3^{2-}]$-based impact on $\delta^{18}O_c$ by applying the regression for both combined species (black in Figure 5a) starting from a high modern deep Atlantic reference value of ∼105 µmol/kg (Yu & Elderfield, 2007), given that the $\delta^{18}O_c$ stack is predominantly Atlantic in nature. We curtail the calculations at a minimum $[CO_3^{2-}]$ limit of 0 µmol/kg, so that the calculations yield the maximum potential impact of the carbonate ion effect, although we note that the minimum $[CO_3^{2-}]$ limit today (in the deep Pacific), is considerably higher at ∼50 µmol/kg (Broecker and Sutherland (2000). The reconstructed maximum $[CO_3^{2-}]$ impacts (red in Figure 6b) are shown with 68% uncertainties bounds (orange) that are based on propagation of the combined $T_{w\_modified}$ uncertainty bounds (Figure 4a) and $[CO_3^{2-}]$ regression prediction intervals (Figure 5a). In Figure 6c, we show inferred deep-water $[CO_3^{2-}]$ for this maximum-impact assessment, with uncertainty bounds. Here we note that, given the continuation (to some variable extent) of carbonate deposition in the world ocean throughout the Cenozoic, extended intervals with carbonate ion concentrations approximating zero are unlikely to have existed in reality. Regardless, even considering the maximum

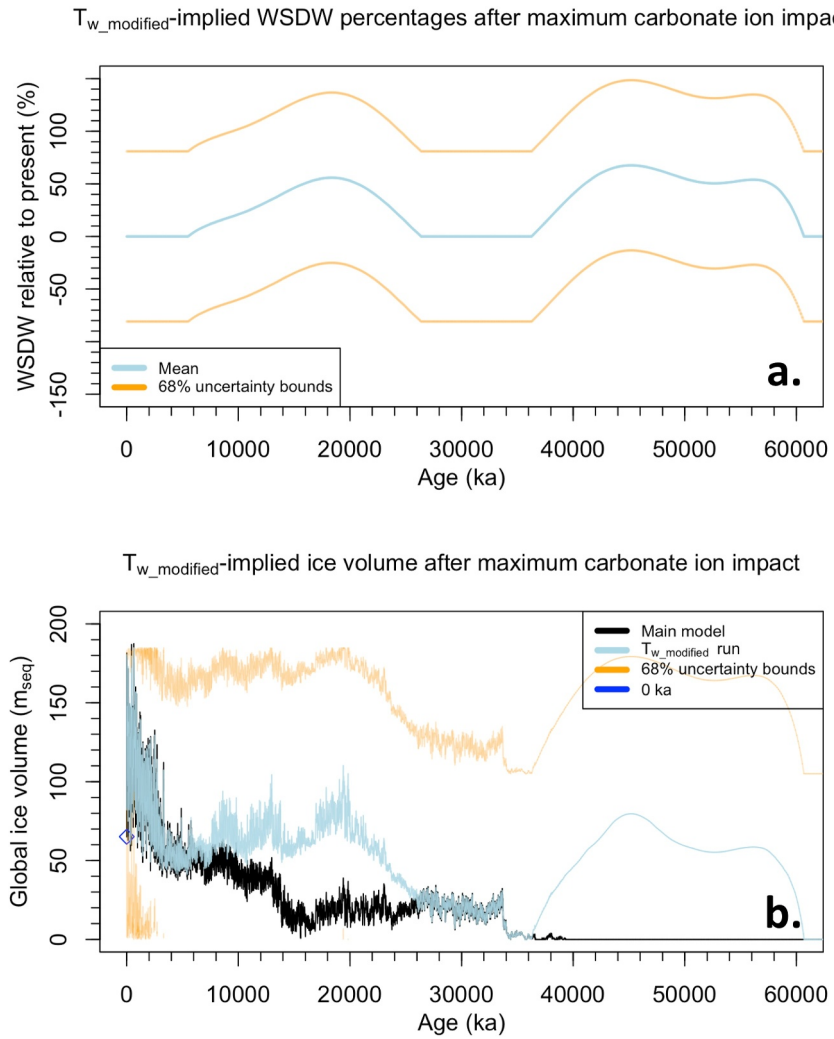

Figure 8. Implied changes in WSDW contribution or ice volume in the main model experiment after allowing for maximum carbonate ion impacts; that is, to explain residual differences between the red and black records in Figure 6b (a) Attributing the remaining offsets entirely to WSDW variations. (b) Attributing the remaining offsets entirely to ice-volume variations. Light blue indicates mean values, and orange lines delimit 68% uncertainty intervals. For comparison, we also show in (b) the initial ice-volume variations in the main model experiment (black).

carbonate ion impacts inferred here leaves obvious residual offsets between the red and black lines in Figure 6b, which means that scenario (*a2*) cannot satisfactorily address the discrepancies between clumped isotope-based T_w (Meckler et al., 2022; their original values) and T_w from $\delta^{18}O_c$ deconvolution, unless pushed toward uncertainty limits. Yet, it is also clear that consideration of plausible [CO_3^{2-}] fluctuations offers considerable potential to reconcile reconstructions if at least one additional major influence could be identified, which offers a more constructive way forward. We revisit the concept of combined effects later, after discussion of scenario (b) and of the potential impacts of different ice-sheet profiles.

3.2. Hypothesis That $\delta^{18}O_w$ and/or Ice Volume Are Understood Insufficiently

Scenario (b), portrayed in Figure 7, provides insight into $\delta^{18}O_{w\_implied}$ (light blue) from the clumped isotope based $\delta^{18}O_{t\_modified}$ (red) and measured $\delta^{18}O_c$ (black). This scenario indicates a strong positive $\delta^{18}O_w$ bias, which—when translated using the loess fit between global ice volume and $\delta^{18}O_w$—produces extreme global ice-volume estimates (Figure 7b, light blue for the clumped isotope-based experiment vs. black for the initial model run). This would suggest that the Miocene, including the Middle Miocene Climate Optimum (MMCO; ~17–12 Ma), was characterized by maximum ice volume, which then decreased toward the Pleistocene and was

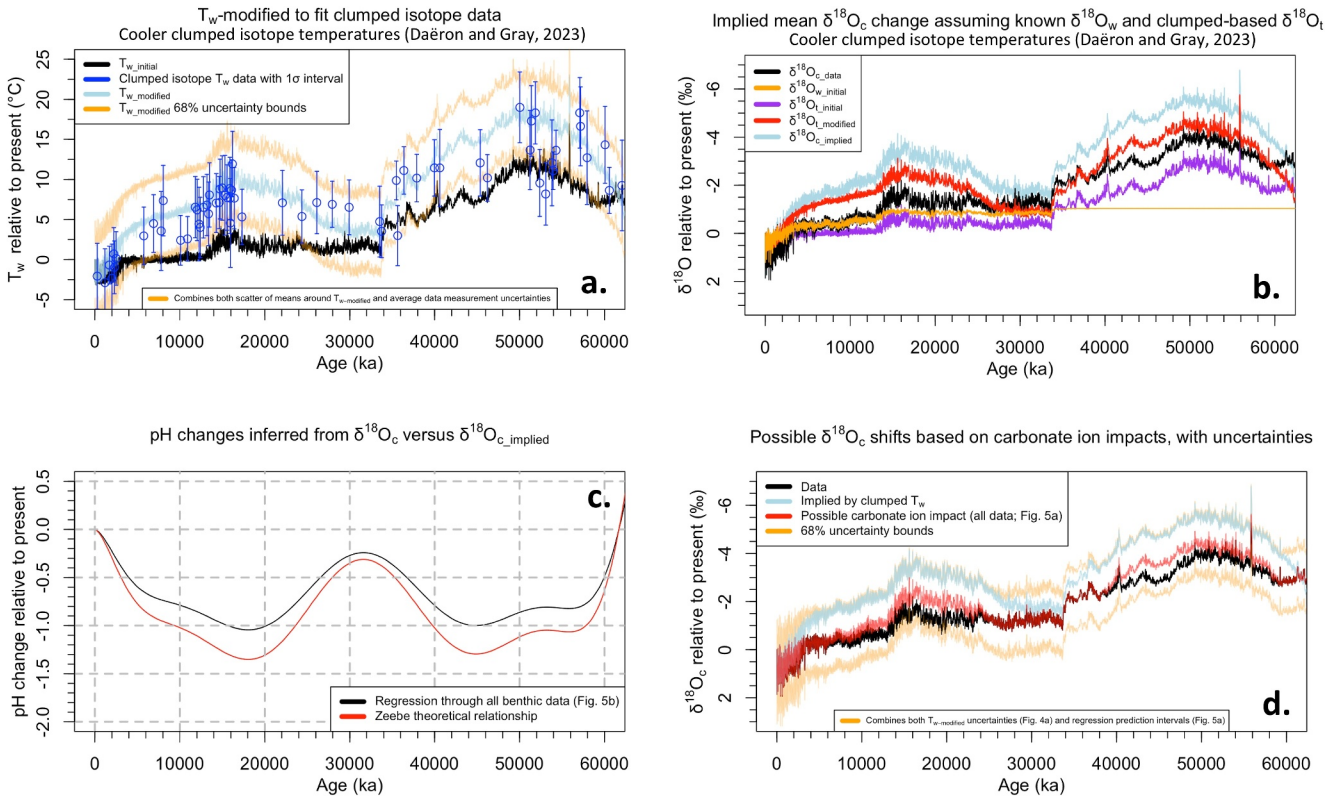

Figure 9. (a) As Figure 4a, but for a model experiment using a cooler clumped isotope temperature calibration (Daëron & Gray, 2023). Note that Taylor et al. (2023), using a similar calibration, find similar T_w change across the Eocene-Oligocene Transition, but in higher resolution. They observe cooling from ~11 to ~6°C in the eastern equatorial Pacific, where modern T_w is about 1.6°C, so that values relative to the present anomaly change from ~9 to ~4°C. (b) As Figure 4b but based on the temperatures from panel (a). (c) As Figure 6a but based on the temperatures from panel (a). (d) As Figure 6b but based on the temperatures from panel (a).

equaled only during the most severe Late Pleistocene ice ages (Figure 7b). In addition, similarly large ice volumes are suggested during the Paleocene-Eocene greenhouse interval (Figure 7b). Ice volume is presented in meters sea-level equivalent, so that sea-level change by first approximation equals negative ice-volume change. Hence, extremely low sea levels are suggested; below −100 m from ~24 to ~6 Ma and between ~60 and 40 Ma. Such an implied global ice-volume/sea-level history makes no sense in view of other data that the global glaciation state increased from the MMCO to the Pleistocene (for overviews, see: Rohling et al., 2021, 2022; Steinthorsdottir et al., 2021) and that little to no ice existed during most of the Paleocene-Eocene. So, might the explanation lie in a radical misunderstanding of Rayleigh Distillation over continental ice sheets? From this perspective, the large positive $\delta^{18}O_{w\_implied}$ (light blue) deviation and its shift in a more negative direction toward the Pleistocene ice ages (Figure 7a) would imply not only a misunderstanding of the Rayleigh Distillation magnitude, but even of its sign. That is, global mean ice-sheet $\delta^{18}O$ would need to have become progressively more positive from the warm MMCO to the Pleistocene ice ages to explain the $\delta^{18}O_{w\_implied}$ drop (Figure 7a). This is contrary to all thermodynamic understanding and laboratory and field observations of how Rayleigh Distillation affects $\delta^{18}O$ (e.g., Ellehoj et al., 2013; Jouzel & Merlivat, 1984; Lamb et al., 2017; Majoube, 1970, 1971; Merlivat, 1978; Merlivat & Jouzel, 1979). Similar to scenario *(a)*, scenario *(b)* therefore also fails to satisfactorily explain the stable oxygen isotope implications of clumped isotope T_w measurements.

3.3. Hypothesis That Large $\delta^{18}O_w$ Variations Can Be Explained by Warm Saline Deep Water

The mean WSDW scenario requires large (>50%) WSDW contributions throughout the Cenozoic, and up to 100% or more between ~22 and ~10 Ma, as well as between ~60 and ~40 Ma (Figure 7c). Values below 0% and over 100% are evidently unrealistic and indicate that the WSDW mechanism by itself cannot explain the $\delta^{18}O_w$ implications of clumped isotope T_w data. Moreover, the generally high WSDW percentages inferred in both scenarios, and the relatively similar values before and after the Eocene-Oligocene Transition at ~34 Ma, when

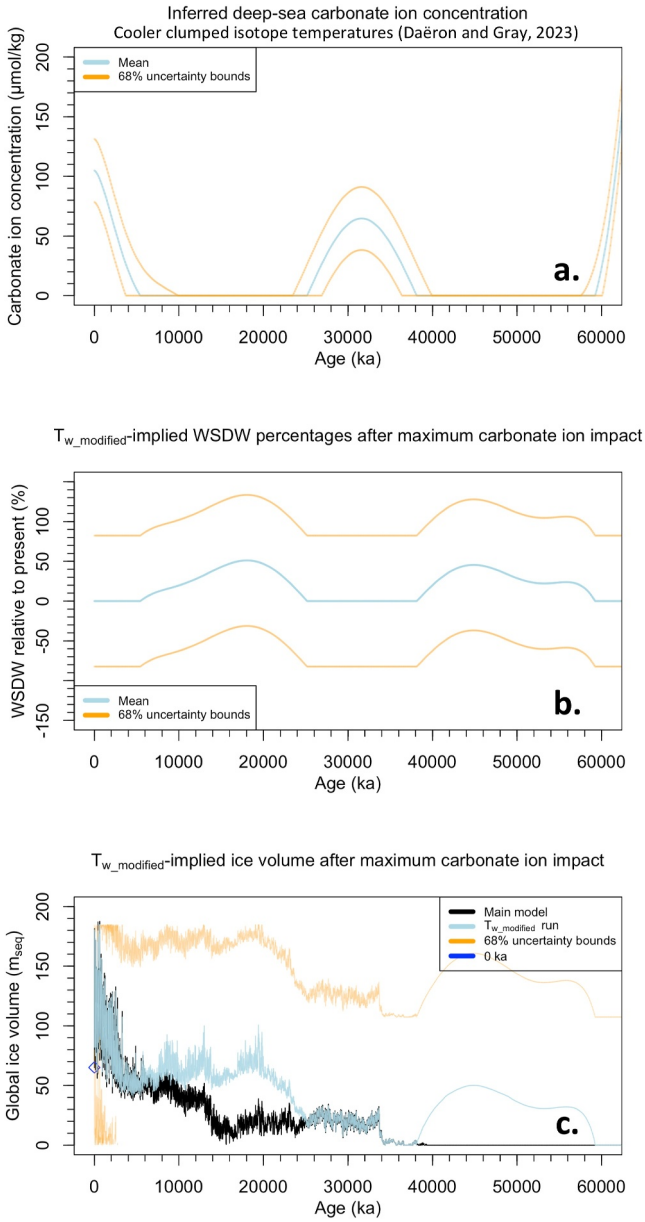

Figure 10. (a) As Figure 6c but based on the temperatures from Figure 9a (b) As Figure 8a but based on the temperatures from Figure 9a (b) As Figure 8b but based on the temperatures from Figure 9a.

Table 2
Surface-Water Density (ρ) Changes for Salinity Reduction From S = 40 to 35 psu, and Cooling From T = 15 to 0°C (Chapman, 2006)

	$S = 40$	$S = 37.5$	$S = 35$
$T = 15$	$\rho = 1.0298$	$\rho = 1.0279$	$\rho = 1.0260$
$T = 10$	$\rho = 1.0309$	$\rho = 1.0289$	$\rho = 1.0270$
$T = 5$	$\rho = 1.0316$	$\rho = 1.0297$	$\rho = 1.0277$
$T = 0$	$\rho = 1.0321$	$\rho = 1.0301$	$\rho = 1.0281$

Note. Units: ρ in kg l^{-1}, S in psu, T in °C.

major Antarctic glaciation occurred, seem unrealistic in view of evidence of high-latitude-focused deep-water formation during the early Oligocene (Liu et al., 2009) and the (at least Southern Hemisphere) development of substantial ice masses (thus, snow cover), which provides a major potential source for summer fresh-water input, which would have reduced surface salinities.

Surface-water density changes for salinity reduction from S = 40 to 35 psu, and cooling from T = 15 to 0°C are shown in Table 2 (Chapman, 2006). If these are used as potential deep-sea densities, then WSDW of T = 10–15°C and S = 37.5 psu could theoretically coexist/mix with cold deep water of T = ~0°C and S = 35 psu. Yet, major contributions to global deep-water volume depend not only on possible water density, but also on the likelihood of sufficient volumes of deep-water production (volume flux). Given that major evaporative basins such as the Mediterranean and Red Sea produce only of order 1 Sverdrup (Sv; 1×10^6 m^3 s^{-1}) of WSDW each, and that no other major WSDW source basins are available under near-modern paleogeographic conditions, the inferred ~30%–70% WSDW contributions to the global deep-water volume in Late Miocene to mid-Pliocene times (Figure 7c) seem unlikely. Moreover, following low-latitude Tethys Ocean closure at ~50 Ma (Zahirovic et al., 2016), except for some Red Sea-Mediterranean connectivity (Bialik et al., 2019), the entire time interval since ~50 Ma at least has lacked likely high-volume WSDW source regions. Hence, the large WSDW contributions inferred throughout the 40–1 Ma interval in Figure 7c seem unrealistic. The WSDW hypothesis to explain large deep-sea $\delta^{18}O_w$ variations (Meckler et al., 2022), therefore, is rejected as a sole explanation. We will revisit this later in the section on combined effects.

3.4. Hypothesis That Ice-Sheet Aspect-Ratio Changes Might Explain the Discrepancies

Rayleigh Distillation impacts of precipitation $\delta^{18}O$ over flatter ice sheets (Figures S4 in Supporting Information S1) are less intense, producing ice sheets with less-negative mean $\delta^{18}O$ values (Figure S5a in Supporting Information S1), which in turn impart less-positive $\delta^{18}O_w$ changes (Figure S5b in Supporting Information S1). Based on these changes, we repeat the hypothesis-testing analyses using the relatively warm Meckler et al. (2022) clumped isotope calibration (Figures S6 and S7 in Supporting Information S1). It appears that considering low-slung, slippery ice sheets does not substantially alter the comparisons between reconstructions using clumped isotope-based T_w data or straightforward ("initial") $\delta^{18}O_c$ deconvolution.

3.5. Impacts of Different Clumped Isotope Calibrations and of Combined Effects

The hypotheses evaluated above all assume that paleotemperatures inferred from clumped isotope data are correct. However, Looser et al. (2023) concluded that: "*our results demonstrate the importance of material-specific kinetic parameters and we urge caution when interpreting Δ_{47}-derived temperatures of biogenic carbonates from deep-time archives*." Yet, careful calibrations by Peral et al. (2018) and Piasecki et al. (2019) suggest that kinetic effect influences on mean clumped isotope-based paleotemperatures of benthic foraminifera may be small, despite spread in individual analyses. Moreover, deep-sea clumped isotope paleotemperatures are not far from Mg/Ca-based paleotemperatures (e.g., Braaten et al., 2023; Leutert et al., 2021; Modestou et al., 2020). While healthy caution remains necessary when

assuming that no complications exist in clumped isotope data, especially from ancient sequences, it is important to note that similar caution applies when assuming that species-specific kinetic effects remained constant through time in stable isotope fractionation (cf. Daëron & Gray, 2023). It seems desirable for future work to constrain such influences in either method, including in applications to ancient sequences.

Regardless, there is a more obvious issue that affects the T_w comparisons made here. Daëron and Gray (2023) re-evaluated clumped isotope temperature calibrations and proposed a different, cooler, planktonic foraminifera-based version. Applied here, that calibration results in an average ∼2.2°C shift to lower reconstructed temperatures, with greater change at the colder end than at the warmer end. As argued before (*Introduction*), we use the Meckler et al. (2022) and Daëron and Gray (2023) calibrations as warm and cold endmembers. Hence, we apply the Daëron and Gray (2023) calibration and revisit the various scenarios evaluated above, both for the experiment with steep ice sheets (Figures 9 and 10) and for the experiment with low-slung ice sheets (Figures S8 and S9 in Supporting Information S1). The lower clumped-isotope temperatures reduce the T_w discrepancy relative to that from $\delta^{18}O_c$ deconvolution (Figure 9a and Figure S8a in Supporting Information S1). Relative to experiments with the relatively warm clumped isotope calibration (Figure 6a and Figure S6c in Supporting Information S1), the range of inferred pH variations is somewhat reduced, now rarely exceeding −1 pH units (Figure 9c and Figure S8c in Supporting Information S1).

Similarly, it appears that combining carbonate ion effects with use of a cooler clumped isotope recalibration can explain a slightly larger portion of the offsets between clumped isotope-based $\delta^{18}O_{c\_implied}$ and measured $\delta^{18}O_c$ (light blue and black, respectively) (see Figure 9d vs. Figure 6b, and Figure S8d vs. Figure S6d in Supporting Information S1; where red indicates the mean record shifted due to carbonate ion variations, and orange indicates 68% uncertainty bounds). Whichever experiment we investigate, however, evaluation of the mean carbonate ion effect leaves some residual discrepancies between ∼24 and ∼12 Ma, and between ∼56 and ∼36 Ma. Given the generous uncertainty bounds, this could be simply dismissed as "unresolved," but we consider it more instructive to consider what these residual discrepancies might imply about additional processes that may have operated in combination with carbonate ion changes. Hence, we quantify the residual discrepancies in terms of either implied WSDW contribution or implied ice volume, both with propagated uncertainties at the 68% level (Figures 8a, 8b, 10b and 10c). Mean WSDW implications reach up to ∼60% for the warm Meckler et al. (2022) calibration (Figure 8a), and lower values for the cool Daëron and Gray (2023) calibration (Figure 10b). In the warm periods in which these WSDW contributions are suggested, such levels might be feasible; this may be tested with future research. In contrast, mean ice-volume implications reach present-day values or greater, which seems unlikely for the warm periods in question (Figures 8b and 10c). We contend that consideration of major carbonate-ion impacts combined with additional WSDW influences may be promising for reconciling clumped isotope T_w records with benthic $\delta^{18}O_c$ records in detail.

3.6. Implications and Future Development

Our reconciliation between deep-sea T_w estimates from benthic $\delta^{18}O_c$ deconvolution and from clumped isotopes contains many simplifications and educated guesses. Yet, it opens a new avenue for internally consistent quantitative understanding of Cenozoic variability in sea level (ice volume), GIA-corrected ice-sheet heights and mean ice $\delta^{18}O$, sea-water $\delta^{18}O$, sea-water $\delta^{18}O$, deep-sea temperature, and deep-sea $[CO_3^{2-}]$ variations (with implications for global pCO_2). Formulation of a more precise and extensively tested framework will require improved modeling, construction of a more globally representative and higher-resolution clumped isotope record, further advances in clumped isotope calibration for benthic foraminifera, addition of other paleotemperature constraints, targeted investigation of potential WSDW admixtures, and long-timescale deep-sea $[CO_3^{2-}]$ reconstruction using benthic foraminiferal B/Ca or deep-sea pH using B isotopes.

4. Conclusions

We present new sea-level (ice-volume) and deep-sea temperature reconstructions based on $\delta^{18}O_c$ deconvolution, and compare these with clumped isotope-based deep-sea temperature data. We find that the results from these two approaches can be reconciled with each other if realistically possible $[CO_3^{2-}]$ or pH influences on $\delta^{18}O_c$ are considered along with modest Warm Saline Deep Water contributions during warm intervals, especially if the clumped isotope-based deep-sea temperatures are obtained using a cooler calibration (e.g., as proposed by Daëron and Gray (2023), although we acknowledge that this is a cold endmember among available calibrations).

Consideration of low-slung ice sheets only marginally affects these findings, and does not seem to be a particularly promising avenue for reconciling clumped isotope T_w records with benthic $\delta^{18}O_c$ records. Our first iteration of an internally consistent suite of Cenozoic variability in sea level (ice volume), GIA-corrected ice-sheet heights and mean ice $\delta^{18}O$, sea-water $\delta^{18}O$, deep-sea temperature, and deep-sea $[CO_3^{2-}]$ variations (with implications for global pCO_2) still is relatively unrefined and Atlantic-focussed due to the origins of both the clumped isotope and $\delta^{18}O_c$ records that are used, but lays a comprehensive foundation for advances through model improvements and additional analytical work.

Data Availability Statement

R-codes, all required input data, and selected output data for the experiments presented in this work are available at Rohling (2024).

Acknowledgments
This study contributes to Australian Research Council Discovery Project DP200101157. We thank M. Ziegler and I. Kocken for valuable discussions on the need to quantitatively contrast methodologies and test hypotheses for any discrepancies, and M. Daëron and two anonymous reviewers for two rounds of high-quality, constructive reviews.

References

Adkins, J. F., McIntyre, K., & Schrag, D. P. (2002). The salinity, temperature, and $\delta^{18}O$ of the glacial deep ocean. *Science*, *298*(5599), 1769–1773. https://doi.org/10.1126/science.1076252

Adkins, J. F., & Schrag, D. P. (2000). Pore fluid constraints on deep ocean temperature and salinity during the Last Glacial Maximum. *Geophysical Research Letters*, *28*(5), 771–774. https://doi.org/10.1029/2000GL011597

Bailey, I., Bolton, C. T., deConto, R. M., Pollard, D., Schiebel, R., & Wilson, P. A. (2010). A low threshold for North Atlantic ice rafting from "low-slung slippery" late Pliocene ice sheets. *Paleoceanography*, *25*(1), PA1212. https://doi.org/10.1029/2009PA001736

Berends, C. J., de Boer, B., & van de Wal, R. S. W. (2021). Reconstructing the evolution of ice sheets, sea level, and atmospheric CO_2 during the past 3.6 million years. *Climate of the Past*, *17*(1), 361–377. https://doi.org/10.5194/cp-17-361-2021

Bialik, O. M., Frank, M., Betzler, C., Zammit, R., & Waldmann, N. D. (2019). Two-step closure of the Miocene Indian ocean gateway to the Mediterranean. *Scientific Reports*, *9*(1), 8842. https://doi.org/10.1038/s41598-019-45308-7

Bigg, G. R., & Rohling, E. J. (2000). An oxygen isotope data set for marine waters. *Journal of Geophysical Research*, *105*(C4), 8527–8535. https://doi.org/10.1029/2000JC900005

Bijma, J., Spero, H. J., & Lea, D. W. (1999). Reassessing foraminiferal stable isotope geochemistry: Impact of the oceanic carbonate system (experimental results). In G. Fischer & G. Wefer (Eds.), *Use of Proxies in Paleoceanography: Examples From the South Atlantic* (pp. 489–512). Springer-Verlag. Retrieved from https://epic.awi.de/id/eprint/341/1/Bij1999a.pdf

Bintanja, R., & van de Wal, R. S. W. (2008). North American ice-sheet dynamics and the onset of 100,000-year glacial cycles. *Nature*, *454*(7206), 869–872. https://doi.org/10.1038/nature07158

Bintanja, R., van de Wal, R. S. W., & Oerlemans, J. (2005). Modelled atmospheric temperatures and global sea level over the past million years. *Nature*, *437*(7055), 125–128. https://doi.org/10.1038/nature03975

Braaten, A. H., Jakob, K. A., Ho, S. L., Friedrich, O., Galaasen, E. V., de Schepper, S., et al. (2023). Limited exchange between the deep Pacific and Atlantic oceans during the warm mid-Pliocene and Marine Isotope Stage M2 "glaciation". *Climate of the Past*, *19*(11), 2109–2125. https://doi.org/10.5194/cp-19-2109-2023

Broecker, W. S., & Sutherland, S. (2000). Distribution of carbonate ion in the deep ocean: Support for a post-little ice age change in Southern ocean ventilation? *Geochemistry, Geophysics, Geosystems*, *1*(7), 1023. https://doi.org/10.1029/2000GC000039

Chapman, R. (2006). A sea water equation of state calculator. https://science.widener.edu/~svanbram/seawater.html

Clark, P. U., & Pollard, D. (1998). Origin of the middle Pleistocene transition by ice sheet erosion of regolith. *Paleoceanography*, *13*, 1–9. https://doi.org/10.1029/97PA02660

Coogan, L. A., Daëron, M., & Gillis, K. M. (2019). Seafloor weathering and the oxygen isotope ratio in seawater: Insight from whole-rock $\delta^{18}O$ and carbonate $\delta^{18}O$ and Δ_{47} from the Troodos ophiolite. *Earth and Planetary Science Letters*, *508*, 41–50. https://doi.org/10.1016/j.epsl.2018.12.014

Coplen, T. B., Kendall, C., & Hopple, J. (1983). Comparison of stable isotope reference samples. *Nature*, *302*(5905), 236–238. https://doi.org/10.1038/302236a0

Cox, K. A., Stanford, J. D., McVicar, A. J., Rohling, E. J., Heywood, K. J., Bacon, S., et al. (2010). Interannual variability of Arctic sea ice export into the East Greenland Current. *Journal of Geophysical Research*, *115*(C12), C12063. https://doi.org/10.1029/2010JC006227

Craig, H., & Gordon, L. I. (1965). Isotope oceanography: Deuterium and oxygen 18 variations in the ocean and the marine atmosphere. In *Symposium on Marine Geochemistry* (Vol. 3, pp. 277–374). University of Rhode Island Occasional Publications.

Daëron, M., & Gray, W. R. (2023). Revisiting Oxygen-18 and clumped isotopes in planktic and benthic foraminifera. *Paleoceanography and Paleoclimatology*, *38*(10), e2023PA004660. https://doi.org/10.1029/2023PA004660

Daëron, M., & Vermeesch, P. (2024). Omnivariant generalized least squares regression: Theory, geochronological applications, and making the case for reconciled Δ_{47} calibrations. *Chemical Geology*, *647*, 121881. https://doi.org/10.1016/j.chemgeo.2023.121881

de Boer, B., van de Wal, R. S. W., Bintanja, R., Lourens, L. J., & Tuenter, E. (2010). Cenozoic global ice-volume and temperature simulations with 1-D ice-sheet models forced by benthic $\delta^{18}O$ records. *Annals of Glaciology*, *51*(55), 23–33. https://doi.org/10.3189/172756410791392736

Eiler, J. M. (2007). "Clumped-isotope" geochemistry—The study of naturally-occurring, multiply-substituted isotopologues. *Earth and Planetary Science Letters*, *262*(3–4), 309–327. https://doi.org/10.1016/j.epsl.2007.08.020

Eiler, J. M. (2011). Paleoclimate reconstruction using carbonate clumped isotope thermometry. *Quaternary Science Reviews*, *30*(25–26), 3575–3588. https://doi.org/10.1016/j.quascirev.2011.09.001

Elderfield, H., Ferretti, P., Greaves, M., Crowhurst, S., McCave, I. N., Hodell, D., & Piotrowski, A. M. (2012). Evolution of ocean temperature and ice volume through the Mid-Pleistocene Climate Transition. *Science*, *337*(6095), 704–709. https://doi.org/10.1126/science.1221294

Elderfield, H., Greaves, M., Barker, S., Hall, I. R., Tripati, A., Ferretti, P., et al. (2010). A record of bottom water temperature and seawater $\delta^{18}O$ for the Southern Ocean over the past 440 kyr based on Mg/Ca of benthic foraminiferal *Uvigerina* spp. *Quaternary Science Reviews*, *29*(1–2), 160–169. https://doi.org/10.1016/j.quascirev.2009.07.013

Ellehoj, M. D., Steen-Larsen, H. C., Johnsen, S. J., & Madsen, M. B. (2013). Ice-vapor equilibrium fractionation factor of hydrogen and oxygen isotopes: Experimental investigations and implications for stable water isotope studies. *Rapid Communications in Mass Spectrometry*, *27*(19), 2149–2158. https://doi.org/10.1002/rcm.6668

Epstein, S., Buchsbaum, R., Lowenstam, H. A., & Urey, H. C. (1951). Carbonate-water isotopic temperature scale. *Geological Society of America Bulletin*, *62*(4), 417–426. https://doi.org/10.1130/0016-7606(1951)62[417:cits]2.0.co;2

Epstein, S., Buchsbaum, R., Lowenstam, H. A., & Urey, H. C. (1953). Revised carbonate-water isotopic temperature scale. *Geological Society of America Bulletin*, *64*(11), 1315–1325. https://doi.org/10.1130/0016-7606(1953)64[1315:RCITS]2.0.CO;2

Erez, J., & Luz, B. (1982). Temperature control of oxygen isotope fractionation of cultured planktonic foraminifera. *Nature*, *297*(5863), 220–222. https://doi.org/10.1038/297220a0

Erez, J., & Luz, B. (1983). Experimental paleotemperature equation for planktonic foraminifera. *Geochimica et Cosmochimica Acta*, *47*(6), 1025–1031. https://doi.org/10.1016/0016-7037(83)90232-6

Gernon, T. M., Hincks, T. K., Merdith, A., Rohling, E. J., Palmer, M. R., Foster, G. L., et al. (2021). Global chemical weathering dominated by continental arcs since the mid-Palaeozoic. *Nature Geoscience*, *14*(9), 690–696. https://doi.org/10.1038/s41561-021-00806-0

Ghosh, P., Adkins, J., Affek, H., Balta, B., Guo, W., Schauble, E. A., et al. (2006). ^{13}C–^{18}O bonds in carbonate minerals: A new kind of paleothermometer. *Geochimica et Cosmochimica Acta*, *70*(6), 1439–1456. https://doi.org/10.1016/j.gca.2005.11.014

Hansen, J., Sato, M., Russell, G., & Kharecha, P. (2013). Climate sensitivity, sea level and atmospheric carbon dioxide. *Philosophical Transactions of the Royal Society of London - A*, *371*(2001), 20120294. https://doi.org/10.1098/rsta.2012.0294

Harmon, R. S., & Schwarcz, H. P. (1981). Changes of ^{2}H and ^{18}O enrichment of meteoric water and Pleistocene glaciation. *Nature*, *290*(5802), 125–128. https://doi.org/10.1038/290125a0c

Herbert, T. D., Dalton, C. A., Liu, Z., Salazar, A., Si, W., & Wilson, D. S. (2022). Tectonic degassing drove global temperature trends since 20 Ma. *Science*, *377*(6601), 116–119. https://doi.org/10.1126/science.abl4353

Hou, S., Stap, L. B., Paul, R., Nelissen, M., Hoem, F. S., Ziegler, M., et al. (2023). Reconciling Southern Ocean fronts equatorward migration with minor Antarctic ice volume change during Miocene cooling. *Nature Communications*, *14*(1), 7230. https://doi.org/10.1038/s41467-023-43106-4

Huntington, K. W., & Petersen, S. V. (2023). Frontiers of carbonate clumped isotope thermometry. *Annual Review of Earth and Planetary Sciences*, *51*(1), 611–641. https://doi.org/10.1146/annurev-earth-031621-085949

Jasechko, S., Birks, S. J., Gleeson, T., Wada, Y., Fawcett, P. J., Sharp, Z. D., et al. (2014). The pronounced seasonality of global groundwater recharge. *Water Resources Research*, *50*(11), 8845–8867. https://doi.org/10.1002/2014WR015809

Jouzel, J., & Merlivat, L. (1984). Deuterium and oxygen 18 in precipitation: Modeling of the isotopic effects during snow formation. *Journal of Geophysical Research*, *89*(D7), 11749–11757. https://doi.org/10.1029/JD089iD07p11749

Kim, S. T., & O'Neil, J. R. (1997). Equilibrium and nonequilibrium oxygen isotope effects in synthetic calcites. *Geochimica et Cosmochimica Acta*, *61*(16), 3461–3475. https://doi.org/10.1016/s0016-7037(97)00169-5

Lamb, K. D., Couser, B. W., Bolot, M., Sarkozy, L., Ebert, V., Saathoff, H., et al. (2017). Laboratory measurements of HDO/H_2O isotopic fractionation during ice deposition in simulated cirrus clouds. *Proceedings of the National Academy of Sciences of the U.S.A.*, *114*, 5612–5617. https://doi.org/10.1073/pnas.1618374114

Lear, C. H., Rosenthal, Y., Coxall, H. K., & Wilson, P. A. (2004). Late Eocene to early Miocene ice sheet dynamics and the global carbon cycle. *Paleoceanography*, *19*(4), PA4015. https://doi.org/10.1029/2004pa001039

Leutert, T. J., Modestou, S., Bernasconi, S. M., & Meckler, A. N. (2021). Southern Ocean bottom-water cooling and ice sheet expansion during the middle Miocene climate transition. *Climate of the Past*, *17*(5), 2255–2271. https://doi.org/10.5194/cp-17-2255-2021

Leutert, T. J., Sexton, P. F., Tripati, A., Piasecki, A., Ho, S. L., & Meckler, A. N. (2019). Sensitivity of clumped isotope temperatures in fossil benthic and planktic foraminifera to diagenetic alteration. *Geochimica et Cosmochimica Acta*, *257*, 354–372. https://doi.org/10.1016/j.gca.2019.05.005

Liu, Z., Pagani, M., Zinniker, D., DeConto, R., Huber, M., Brinkhuis, H., et al. (2009). Global cooling during the Eocene-Oligocene climate transition. *Science*, *323*(5918), 1187–1190. https://doi.org/10.1126/science.1166368

Looser, N., Petschnig, P., Hemingway, J. D., Fernandez, A., Morales Grafulha, L., Perez-Huerta, A., et al. (2023). Thermally-induced clumped isotope resetting in belemnite and optical calcites: Towards material-specific kinetics. *Geochimica et Cosmochimica Acta*, *350*, 1–15. https://doi.org/10.1016/j.gca.2023.03.030

Majoube, M. (1970). Fractionation factor of ^{18}O between water vapor and ice. *Nature*, *226*(5252), 1242. https://doi.org/10.1038/2261242a0

Majoube, M. (1971). Fractionnement en oxygène 18 et en deutérium entre l'eau et sa vapeur. *Journal de Chimie Physique*, *10*, 1423–1436. https://doi.org/10.1051/jcp/1971681423

Marchitto, T. M., Curry, W. B., Lynch-Stieglitz, J., Bryan, S. P., Cobb, K. M., & Lund, D. C. (2014). Improved oxygen isotope temperature calibrations for cosmopolitan benthic foraminifera. *Geochimica et Cosmochimica Acta*, *130*, 1–11. https://doi.org/10.1016/j.gca.2013.12.034

Matthews, K. J., Maloney, K. T., Zahirovic, S., Williams, S. E., Seton, M., & Müller, R. D. (2016). Global plate boundary evolution and kinematics since the late Paleozoic. *Global and Planetary Change*, *146*, 226–250. https://doi.org/10.1016/j.gloplacha.2016.10.002

McCrea, J. M. (1950). On the isotopic chemistry of carbonates and a paleotemperature scale. *Journal of Chemical Physics*, *18*(6), 849–857. https://doi.org/10.1063/1.1747785

Meckler, A. N., Sexton, P. F., Piasecki, A. M., Leutert, T. J., Marquardt, J., Ziegler, M., et al. (2022). Cenozoic evolution of deep ocean temperature from clumped isotope thermometry. *Science*, *377*(6601), 86–90. https://doi.org/10.1126/science.abk0604

Merlivat, L. (1978). The dependence of bulk evaporation coefficients on air-water interfacial conditions as determined by the isotopic method. *Journal of Geophysical Research*, *83*(C6), 2977–2980. https://doi.org/10.1029/JC083iC06p02977

Merlivat, L., & Jouzel, J. (1979). Global climatic interpretation of the deuterium-oxygen 18 relationship for precipitation. *Journal of Geophysical Research*, *84*(C8), 5029–5033. https://doi.org/10.1029/JC084iC08p05029

Miller, M. D., Simons, M., Adkins, J. F., & Minson, S. E. (2015). The information content of pore fluid $\delta^{18}O$ and $[Cl^{-}]$. *Journal of Physical Oceanography*, *45*(8), 2070–2094. https://doi.org/10.1175/jpo-d-14-0203.1

Modestou, S. E., Leutert, T. J., Fernandez, A., Lear, C. H., & Meckler, A. N. (2020). Warm middle Miocene Indian Ocean bottom water temperatures: Comparison of clumped isotope and Mg/Ca-based estimates. *Paleoceanography and Paleoclimatology*, *35*(11), e2020PA003927. https://doi.org/10.1029/2020pa003927

NIST. (1992). *Report of investigation, reference materials 8543-8546* (p. 2). National Institute of Standards and Technology, United States Department of Commerce.

O'Neil, J. R., Clayton, R. N., & Mayeda, T. K. (1969). Oxygen isotope fractionation on divalent metal carbonates. *Journal of Chemical Physics*, *51*(12), 5547–5558. https://doi.org/10.1063/1.1671982

Peral, M., Daëron, M., Blamart, D., Bassinot, F., Dewilde, F., Smialkowski, N., et al. (2018). Updated calibration of the clumped isotope thermometer in planktonic and benthic foraminifera. *Geochimica et Cosmochimica Acta*, *239*, 1–16. https://doi.org/10.1016/j.gca.2018.07.016

Piasecki, A., Bernasconi, S. M., Grauel, A.-L., Hannisdal, B., Ho, S. L., Leutert, T. J., et al. (2019). Application of clumped isotope thermometry to benthic foraminifera. *Geochemistry, Geophysics, Geosystems*, *20*(4), 2082–2090. https://doi.org/10.1029/2018GC007961

Pierre, C. (1999). The oxygen and carbon isotope distribution in Mediterranean water masses. *Marine Geology*, *153*(1–4), 41–55. https://doi.org/10.1016/S0025-3227(98)00090-5

Pierre, C., Vergnaud-Grazzini, C., Thouron, D., & Saliège, J.-F. (1986). Compositions isotopiques de l'oxygène et du carbone des masses d'eau en Méditerranée. *Memorie della Societa Geologica Italiana*, *36*, 165–174.

Rohling, E. J. (1994). Glacial conditions in the Red Sea. *Paleoceanography*, *9*(5), 653–660. https://doi.org/10.1029/94PA01648

Rohling, E. J. (2024). Rohling et al PandP second revision_R-codes with input files; and core-top delta18O delta13C data file [Software]. *Figshare*. https://doi.org/10.6084/m9.figshare.27211626

Rohling, E. J., & Bigg, G. R. (1998). Paleo-salinity and $\delta^{18}O$: A critical assessment. *Journal of Geophysical Research*, *103*(C1), 1307–1318. https://doi.org/10.1029/97JC01047

Rohling, E. J., & Cooke, S. (1999). Stable oxygen and carbon isotope ratios in foraminiferal carbonate, chapter 14. In B. K. Sen Gupta (Ed.), *Modern Foraminifera* (pp. 239–258). Kluwer Academic. https://doi.org/10.1007/0-306-48104-9_14

Rohling, E. J., Foster, G. L., Gernon, T. M., Grant, K. M., Heslop, D., Hibbert, F. D., et al. (2022). Comparison and synthesis of sea-level and deep-sea temperature variations over the past 40 million years. *Reviews of Geophysics*, *60*(4), e2022RG000775. https://doi.org/10.1029/2022RG000775

Rohling, E. J., Yu, J., Heslop, D., Foster, G. L., Opdyke, B., & Roberts, A. P. (2021). Sea-level and deep-sea temperature reconstructions suggest quasi-stable states and critical transitions over the past 40 million years. *Science Advances*, *7*(26), eabf5326. https://doi.org/10.1126/sciadv.abf5326

Shackleton, N. J. (1974). Attainment of isotopic equilibrium between ocean water and the benthonic foraminifera genus *Uvigerina*: Isotopic changes in the ocean during the last glacial. *CNRS, Colloques Internationaux du C.N.R.S.*, *219*, 203–209.

Shackleton, N. J., & Opdyke, N. D. (1973). Oxygen isotope and palaeomagnetic stratigraphy of Equatorial Pacific core V28-238: Oxygen isotope temperatures and ice volumes on a 10^5 year and 10^6 year scale. *Quaternary Research*, *3*(1), 39–55. https://doi.org/10.1016/0033-5894(73)90052-5

Spratt, R. M., & Lisiecki, L. E. (2016). A Late Pleistocene sea level stack. *Climate of the Past*, *12*(4), 1079–1092. https://doi.org/10.5194/cp-12-1079-2016

Steinthorsdottir, M., Coxall, H. K., de Boer, A. M., Huber, M., Barbolini, N., Bradshaw, C. D., et al. (2021). The Miocene: The future of the past. *Paleoceanography and Paleoclimatology*, *36*(4), e2020PA004037. https://doi.org/10.1029/2020pa004037

Taylor, V. E., Wilson, P. A., Bohaty, S. M., & Meckler, A. N. (2023). Transient deep ocean cooling in the eastern equatorial Pacific Ocean at the Eocene-Oligocene Transition. *Paleoceanography and Paleoclimatology*, *38*(8), e2023PA004650. https://doi.org/10.1029/2023PA004650

Urey, H. C. (1947). The thermodynamic properties of isotopic substances. *Journal of the Chemical Society*, *1947*, 562–581. https://doi.org/10.1039/jr9470000562

van den Broek, M. (2006). *Constraints from ice dynamics for ice load histories from GIA data of the last ice age, and evidence from GIA data for glaciation of the North Sea Basin* (p. 109). Delft University of Technology Masters thesis. Retrieved from https://repository.tudelft.nl/islandora/object/uuid%3A5bfe26e3-f3cd-4445-afe9-159e6b8beff3

Wadley, M. R., Bigg, G. R., Rohling, E. J., & Payne, A. J. (2002). On modelling present day and last glacial maximum oceanic $\delta^{18}O$ distributions. *Global and Planetary Change*, *32*(2–3), 89–109. https://doi.org/10.1016/S0921-8181(01)00084-4

Westerhold, T., Marwan, N., Drury, A. J., Liebrand, D., Agnini, C., Anagnostou, E., et al. (2020). An astronomically dated record of Earth's climate and its predictability over the last 66 million years. *Science*, *369*(6509), 1383–1387. https://doi.org/10.1126/science.aba6853

Willeit, M., Ganopolsky, A., Calov, R., & Brovkin, V. (2019). Mid-Pleistocene transition in glacial cycles explained by declining CO_2 and regolith removal. *Science Advances*, *5*(4), eaav7337. https://doi.org/10.1126/sciadv.aav7337

Young, A., Flament, N., Maloney, K., Williams, S., Matthews, K., Zahirovic, S., & Müller, R. D. (2019). Global kinematics of tectonic plates and subduction zones since the late Paleozoic Era. *Geoscience Frontiers*, *10*(3), 989–1013. https://doi.org/10.1016/j.gsf.2018.05.011

Yu, J. M., & Elderfield, H. (2007). Benthic foraminiferal B/Ca ratios reflect deep water carbonate saturation state. *Earth and Planetary Science Letters*, *258*(1–2), 73–86. https://doi.org/10.1016/j.epsl.2007.1003.1025

Yu, J., & Elderfield, H. (2008). Mg/Ca in the benthic foraminifera *Cibicidoides wuellerstorfi* and *Cibicidoides mundulus*: Temperature versus carbonate ion saturation. *Earth and Planetary Science Letters*, *276*(1–2), 129–139. https://doi.org/10.1016/j.epsl.2008.09.015

Zahirovic, S., Matthews, K. J., Flament, N., Müller, R. D., Hill, K. C., Seton, M., & Gurnis, M. (2016). Tectonic evolution and deep mantle structure of the eastern Tethys since the latest Jurassic. *Earth-Science Reviews*, *162*, 293–337. https://doi.org/10.1016/j.earscirev.2016.09.005

Zeebe, R. E. (1999). An explanation of the effect of seawater carbonate concentration on foraminiferal oxygen isotopes. *Geochimica et Cosmochimica Acta*, *63*(13–14), 2001–2007. https://doi.org/10.1016/S0016-7037(99)00091-5

Zeebe, R. E. (2001). Seawater pH and isotopic paleotemperatures of Cretaceous oceans. *Palaeogeography, Palaeoclimatology, Palaeoecology*, *170*(1–2), 49–57. https://doi.org/10.1016/S0031-0182(01)00226-7

References From the Supporting Information

Alduchov, O. A., & Eskridge, R. E. (1996). Improved Magnus form approximation of saturation vapor pressure. *Journal of Applied Meteorology*, *35*(4), 601–609. https://doi.org/10.1175/1520-0450(1996)035%3C0601:IMFAOS%3E2.0.CO;2

Abe-Ouchi, A., & Otto-Bliesner, B. (2009). Ice sheet-climate interactions during the ice age cycle. *PAGES News*, *17*(2), 73–74. https://doi.org/10.22498/pages.17.2.73

Dansgaard, W. (1964). Stable isotopes in precipitation. *Tellus*, *16*(4), 436–468. https://doi.org/10.1111/j.2153-3490.1964.tb00181.x

Erokhina, O., Rogozhina, I., Prange, M., Bakker, P., Bernales, J., Paul, A., & Schulz, M. (2017). Dependence of slope lapse rate over the Greenland ice sheet on background climate. *Journal of Glaciology*, *63*(239), 568–572. https://doi.org/10.1017/jog.2017.10

Garlick, G. D. (1974). The stable isotopes of oxygen, carbon, hydrogen in the marine environment. In E. D. Goldberg (Ed.), *The Sea* (Vol. 5, pp. 393–425). John Wiley and Sons.

Hut, G. (1987). *Stable isotope reference samples for geochemical and hydrological investigations*. Consultants Group Meeting, 16 –18.09.1985 (p. 42). International Atomic Energy Agency (I.A.E.A.). https://inis.iaea.org/search/search.aspx?orig_q=RN:18075746

Inglis, G. N., Farnsworth, A., Lunt, D., Foster, G. L., Hollis, C. J., Pagani, M., et al. (2015). Descent toward the icehouse: Eocene sea surface cooling inferred from GDGT distributions. *Paleoceanography*, *30*(7), 1000–1020. https://doi.org/10.1002/2014PA002723

Martin, P. J., & Peel, D. A. (1978). The spatial distribution of 10 m temperatures in the Antarctic Peninsula. *Journal of Glaciology*, *20*(83), 311–317. https://doi.org/10.3189/S0022143000013861

Phillips, C. (2016). http://charlie.weathertogether.net/tag/adiabatic-lapse-rate/

Rohling, E. J. (1999). Environmental controls on Mediterranean salinity and $\delta^{18}O$. *Paleoceanography*, *14*(6), 706–715. https://doi.org/10.1029/1999PA900042

Schmidt, G. A., Bigg, G. R., & Rohling, E. J. (1999). Global seawater oxygen-18 database. http://www.giss.nasa.gov/data/o18data/

Seki, O., Schmidt, D. N., Schouten, S., Hopmans, E. C., Sinninghe Damsté, J. S., & Pancost, R. D. (2012). Paleoceanographic changes in the eastern equatorial Pacific over the last 10 Myr. *Paleoceanography and Paleoclimatology*, *27*(3), PA3224. https://doi.org/10.1029/2011PA002158

Vermeersen, L. L. A., & Schotman, H. H. A. (2009). Constraints on glacial isostatic adjustment from GOCE and sea level data. *Pure and Applied Geophysics*, *166*(8–9), 1261–1281. https://doi.org/10.1007/s00024-004-0503-3

Yu, J., Anderson, R. F., Jin, Z., Rae, J. W. B., Opdyke, B. N., & Eggins, S. M. (2013). Responses of the deep ocean carbonate system to carbon reorganization during the last glacial-interglacial cycle. *Quaternary Science Reviews*, *76*, 39–52. https://doi.org/10.1016/j.quascirev.2013.06.020